

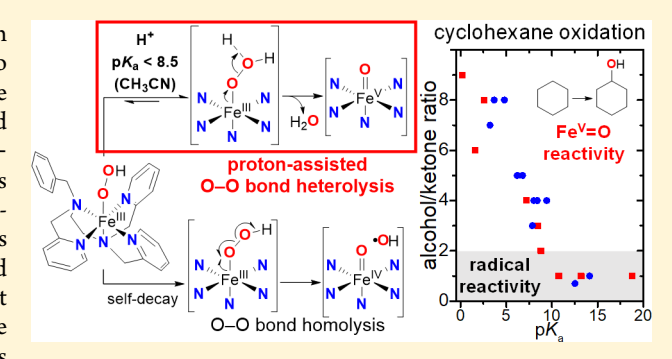
Acid pK_a Dependence in O-O Bond Heterolysis of a Nonheme Fe^{III}-OOH Intermediate To Form a Potent Fe^V=O Oxidant with Heme Compound I-Like Reactivity

Shuangning Xu, Apparao Draksharapu, Waqas Rasheed, and Lawrence Que, Jr. *

Department of Chemistry and Center for Metals in Biocatalysis, University of Minnesota, 207 Pleasant Street SE, Minneapolis, Minnesota 55455, United States

Supporting Information

ABSTRACT: Protons play essential roles in natural systems in controlling O-O bond cleavage of peroxoiron(III) species to give rise to the high-valent iron oxidants that carry out the desired transformations. Herein, we report kinetic and mechanistic evidence that acids can control the mode of O-O bond cleavage for a nonheme $S = 1/2 \text{ Fe}^{\text{III}}$ -OOH species $[(BnTPEN)Fe^{III}(OOH)]^{2+}$ (2, BnTPEN = N-benzyl-N,N',N'tris(2-pyridylmethyl)-1,2-diaminoethane). Addition of acids having pK_a values of >8.5 in CH₃CN results in O-O bond homolysis, leading to the formation of hydroxyl radicals that give rise to alcohol/ketone (A/K) ratios of around 1 in the oxidation of cyclohexane. However, the introduction of acids



with p K_a values of <8.5 elicits a different outcome, namely the achievement of A/K ratios of as high as 9, the observation of rapid and catalytic hydroxylation of cyclohexane, and a million-fold acceleration in the decay rate of the Fe^{III}-OOH intermediate at −40 °C. These results implicate the generation of a highly reactive Fe^V=O species via proton-assisted O-O bond heterolysis of the Fe^{III}-OOH intermediate, which is unprecedented for nonheme iron complexes supported by neutral pentadentate ligands and serves as a nonheme analogue for heme enzyme compounds I.

INTRODUCTION

Iron-containing enzymes are versatile catalysts that utilize oxygen to carry out a variety of oxidative transformations, the most challenging of which is the functionalization of very strong C-H bonds. 1-5 Activation of these inert C-H bonds through hydrogen atom transfer (HAT) is often accomplished by high-valent iron-oxo species, which can be generated by cleaving the O-O bonds of corresponding peroxoiron intermediates derived from O2 or H2O2. One of the best characterized high-valent species is generated by hemecontaining enzymes and known as "compound I" (Cpd I),6 an Fe^{IV}(O)(por^{•+}) species proposed to be the active oxidant in the catalytic cycles of peroxidases and cytochromes P450 (Scheme 1).^{7,8} Its precursor, called "compound 0" (Cpd 0), is an $S = 1/2 \text{ Fe}^{\text{III}}$ -OOH species that gives rise to Cpd I through heterolytic scission of its O-O bond. 9-12 This key step requires the participation of one proton to allow the distal oxygen to leave as water. For H2O2-utilizing heme peroxidases, introduction of the proton to the distal oxygen is proposed to be accomplished by amino acid residue pairs, which serve as general acid-base catalysts and are located at the distal pockets of the heme active sites of the enzymes. 13-16 For dioxygenutilizing cytochrome P450-type enzymes, threonine has been identified as the key residue in the proton delivery networks required to generate Cpd 0 and Cpd I. 17-20

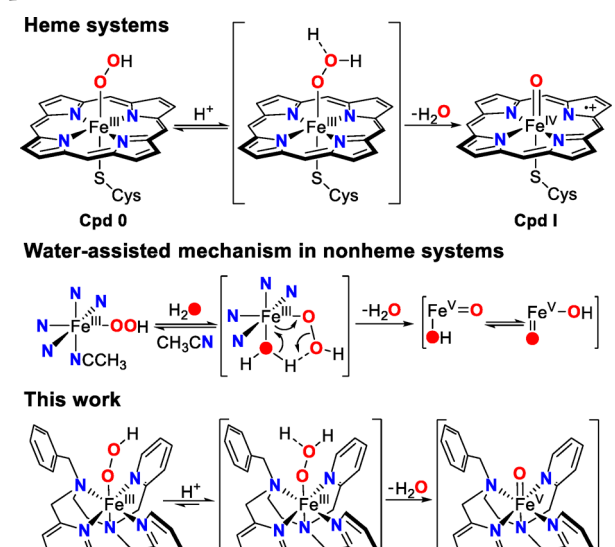
How a proton is involved in the activation of ferric hydroperoxo species remains a fundamental mechanistic question that needs further investigation. Although there are extensive studies on the O-O bond cleavage of heme ferric acylperoxo and alkylperoxo complexes,²¹ there are only a few reports that elucidate the effect of protons on heme FeIII-OOH species, and most only provide indirect evidence by either tracking the hydroperoxo-derived high-valent iron species or the outcome of oxidation reactions. 22-24 Van Eldik and co-workers have studied an Fe^{III}-OOH species supported by an octa-anionic porphyrin ligand in aqueous medium and found that the outcome of O-O bond cleavage switches at pH 8.5, forming either the two-electron oxidized Cpd I at lower pH or the one-electron oxidized Fe^{IV}(O) species at higher pH.²⁴ A similar behavior is observed for the manganese counterpart of Cpd 0 in a study by Groves and co-workers, where it is suggested that the protonation and release of the distal oxygen as water occur concomitantly with the formation of the Mn^V(O) species.²⁵

In nonheme iron systems, the action of the anticancer drug bleomycin (BLM) has been found to involve an S = 1/2 Fe^{III}-OOH species known as activated bleomycin (ABLM), which is proposed to initiate double-stranded DNA cleavage by

Received: August 5, 2019 Published: September 12, 2019



Scheme 1. Proposed Mechanism for Proton-Assisted Activation of the O-O Bonds of Hydroperoxoiron(III) **Species**



attacking the C4'-H bond of the target nucleotide in DNA. $^{26-28}$ However, to what extent the mechanism of action for this Fe^{III}-OOH species parallels that of its heme counterpart Cpd 0 remains unclear. While calculations show that protonation of the peroxo moiety can lower the barrier for O-O bond cleavage and promote the formation of high-valent iron species, 29 it has been suggested that direct HAT by this nonheme Fe^{III}-OOH intermediate may be the most favorable pathway for initiating double-stranded DNA cleavage. 30-3

Many of the synthetic nonheme Fe^{III}-OOH complexes reported thus far are those supported by neutral pentadentate ligands such as N4Py (N4Py = N_1N -bis(2-pyridylmethyl)-Nbis(2-pyridyl)methylamine) and R-TPEN (R-TPEN = N-R- $N_1N'_1N'$ -tris(2-pyridylmethyl)-1,2-diaminoethane), which are generated by adding a large excess of H_2O_2 to their iron(II) precursors at low temperatures. These Fe^{III} –OOH species themselves have been described as "sluggish oxidants" of hydrocarbons, 42 and the lack of oxidative selectivity exhibited by these species has often been attributed to the action of hydroxyl radicals generated via homolysis of the O-O bond of the Fe^{III}-OOH intermediate. 41-44 Currently, experimental evidence for proton-assisted O-O bond heterolysis of nonheme Fe^{III}-OOH species has been found only for those supported by tetradentate ligands such as TPA (TPA = tris(pyridyl-2-methyl)amine) and Me2PyTACN (Me2PyTACN = 1,4-dimethyl-7-(2-pyridylmethyl)-1,4,7-triazacyclononane). For these complexes, the availability of an additional coordination site allows water to bind cis to the hydroperoxo ligand and promote the heterolytic cleavage of the O-O bond via a so-called "water-assisted" mechanism to generate a potent Fe^V(O)(OH) oxidant (Scheme 1).⁴⁵⁻⁵⁴ More recent studies on two other tetradentate ligand complexes, namely [(PyNMe₃)Fe^{III}(OOH)]²⁺ (PyNMe₃ = 3,6,9-trimethyl-3,6,9-triaza-1(2,6)-pyridina-cyclodecaphane) and $[(\beta\text{-BPMCN})\text{Fe}^{\text{III}}(\text{OOH})]^{2+}$ $(\beta\text{-BPMCN} = N, N'\text{-bis-}$ (pyridyl-2-methyl)-N,N'-dimethyl-trans-1,2-diaminocyclohexane), indicate that O-O bond cleavage can be facilitated by strong acids to form Fe^V=O species. 55,56 While the specific role the sixth site plays in the O-O bond cleavage step and the

precise formulation of the actual oxidant remain unclear, these observations strongly suggest that protons may also play a crucial role in O-O bond cleavage in nonheme iron chemistry.

In our continuing effort to elucidate the role protons may play in O-O bond cleavage of Fe^{III}-OOH species, we have turned to the previously well-characterized [(BnTPEN)- $Fe^{III}(OOH)$ ²⁺ complex (2, BnTPEN = N-benzyl-N,N',N'tris(2-pyridylmethyl)-1,2-diaminoethane)35,36,38 and investigated the effect of adding various acids on the fate of the Fe^{III}-OOH species. We demonstrate that the mode of O-O bond cleavage depends on the pK_a value of the added acid and present indirect evidence for the formation of an unprecedented $\lceil (BnTPEN)Fe^{V}(O) \rceil^{3+}$ species via acid-assisted O-O bond heterolysis (Scheme 1), which is capable of facile hydroxylation of saturated hydrocarbons as well as benzene. This study on the effect of adding acid to the metastable Fe^{III}– OOH species may shed light on the mechanisms of protondependent formation of high-valent iron-oxo species in nature.

■ RESULTS AND DISCUSSION

Formation of 2 with HOAc and H₂O₂ at 25 °C. Intermediate 2 can be generated by the reaction of [(BnTPEN)Fe^{II}(OTf)](OTf) (1) with excess H₂O₂ in methanol or acetone as previously reported;⁵⁷ these are conditions typical for the formation of Fe^{III}-OOH species supported by pentadentate ligands. 41 Its formation is associated with the appearance of an absorption maximum at 525 nm arising from a peroxo-to-iron(III) charge-transfer transition³³ and an EPR signal with g = 2.22, 2.16, and 1.96 that is typical of an S = 1/2 Fe^{III} center.⁵⁷ In the absence of other additives, a large excess of H₂O₂ (100 equiv) is needed to obtain a maximum absorbance of ~0.3 from a 1 mM solution of the ferrous precursor in CH₃CN at 25 °C (Figure S1). Under these conditions, the EPR spectrum of this solution shows a mixture of the desired Fe^{III}-OOH intermediate 2 and the corresponding Fe^{III} -OH complex (g = 2.40, 2.18, and 1.90),³³ together accounting for only about 20% of the iron in solution based on double integration of the low-spin signals (Figure S1). However, we have found that the addition of 10 equiv of HOAc (p $K_a = 23.5$ in CH₃CN) to the solution prior to the introduction of H₂O₂ allows 2 to be generated using only 10 equiv of 90% H₂O₂ at an amount representing about 50% of the iron in the reaction mixture with no evidence for any other low-spin ferric moieties in the EPR spectrum (Figure S1). This species exhibits a somewhat sharper UV-vis spectrum with about twice as large an absorbance of ~0.6 at 525 nm (Figure 1. The absence of other S = 1/2 ferric species under these conditions has enabled us to reliably quantify the S = 1/2 EPR signals of 2 and establish an extinction coefficient of 1100 M⁻¹ cm⁻¹ at 525 nm when used in conjunction with the UV-vis absorption spectrum of the same sample (Figure 1, Figure S1). To the best of our knowledge, this result represents the first time that a molar extinction coefficient has been determined for 2, which agrees well with the value of 1000 M⁻¹ cm⁻¹ at 520 nm for the related [(MeTPEN)Fe^{III}(OOH)]²⁺ species (MeTPEN = N-methyl-N,N',N'-tris(2-pyridylmethyl)-1,2-diaminoethane) as determined by Banse and co-workers.

This notable change in speciation prompted us to further investigate what role acetic acid may play in this chemistry. In our efforts, we determined that ¹H NMR spectroscopy should be quite a useful tool for addressing this question. The ¹H NMR spectrum of 1 in CD₃CN only shows features in the diamagnetic region (Figure 2b), which are broader than those

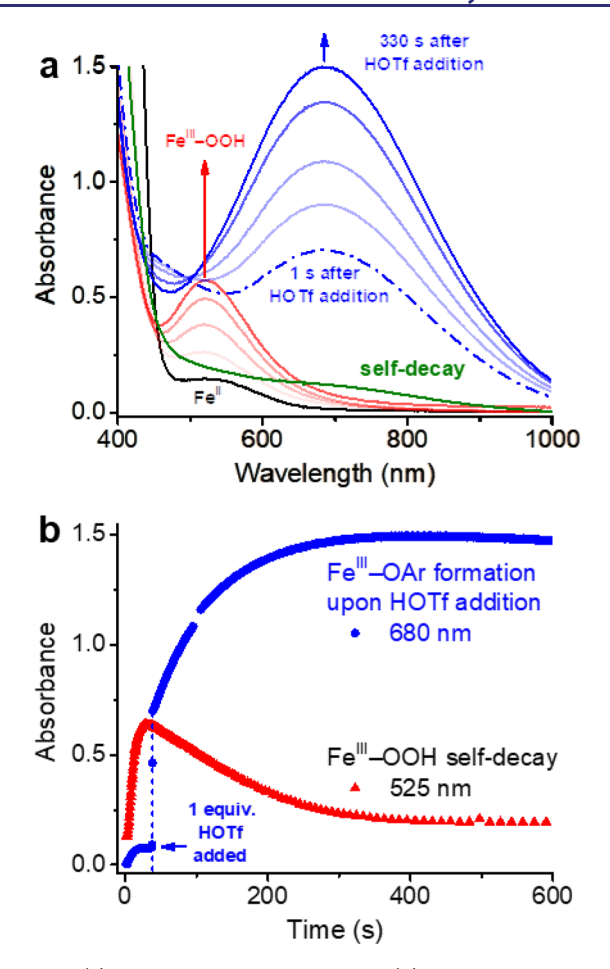


Figure 1. (a) UV-vis spectral changes and (b) time traces associated with the formation and self-decay of 2 in the presence of HOAc (red) and the reaction of 2 with 1 equiv HOTf to form 3 (blue). Reaction conditions: 10 equiv of 90% H₂O₂ is added to 1 mM 1 (black) in CH₃CN in the presence of 10 equiv of HOAc; 1 equiv of HOTf was introduced to this reaction mixture ~30 s after H₂O₂ addition in CH₃CN at 25 °C.

of the free ligand (Figure 2a). This broadening is likely the result of a rapid equilibrium between the predominant diamagnetic low-spin $(S = 0) [Fe^{II}(BnTPEN)(NCCD_3)]^{2+}$ complex in solution⁵⁹ and a minor amount of the paramagnetic high-spin (S = 2) [Fe^{II}(BnTPEN)(OTf)]⁺ species.⁶⁰ In contrast, the NMR spectrum of 1 in CD₂Cl₂ (Figure 2e) shows much broader peaks spread over a much larger chemical shift range, as would be expected for the high-spin (S = 2)[Fe^{II}(BnTPEN)(OTf))]⁺ complex.

No significant change in chemical shifts or line widths is observed when 10 equiv of HOOCCD3 is added to a solution of 1 in CD₃CN, suggesting that acetic acid has no significant effect on the S = 0/S = 2 equilibrium (Figure 2c). However, there is a new peak at ~9 ppm (Figure 2c), which corresponds to the OH proton of acetic acid (Figure S2). Under these conditions, there is also no evidence for the dissociation of a pyridyl arm. However, evidence for pyridyl arm dissociation is observed upon addition of 1 equiv of DClO₄, where a doublet at 8.5 ppm corresponding to the α -pyridyl proton of the dissociated arm appears (Figure 2d and S2). Thus, the BnTPEN ligand remains pentadentate in 1 in the presence of 10 equiv of acetic acid in CD₃CN, and the iron(II) complex has only one available coordination site.

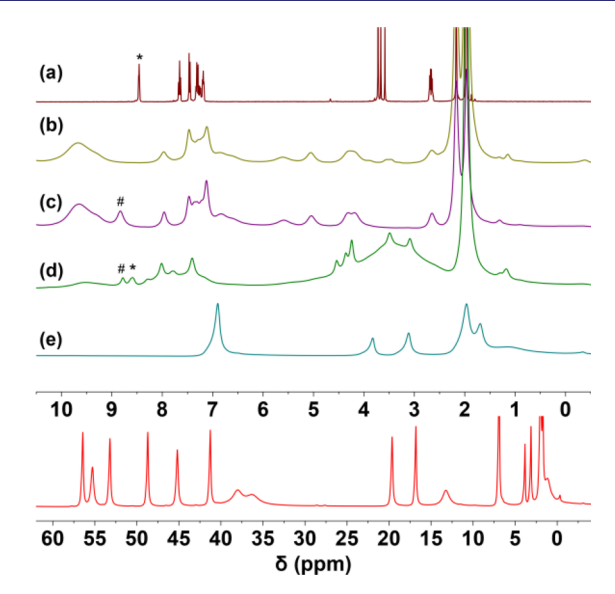
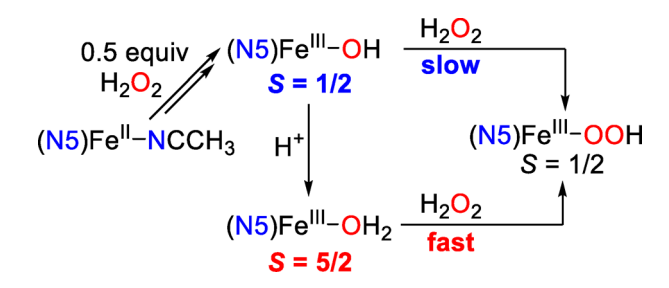


Figure 2. (Top) ${}^{1}H$ NMR spectra in the range of +10.5 to -0.5 ppm in CD₃CN (unless specified otherwise) of (a) the BnTPEN ligand, (b) 2.5 mM 1, (c) (b) + 25 mM CD₃COOH, (d) (b) + 10 mM CD₃COOH and 6 mM DClO₄, and (e) 2.5 mM 1 in CD₂Cl₂. (Bottom) ¹H NMR spectrum of 2.5 mM 1 in CD₂Cl₂ in the range of 62 to -4 ppm. # indicates the OH signal from CD₃COOH. * indicates the α -H signal of a dissociated pyridyl arm upon acidification; see Figure S2 for more spectra illustrating this feature.

As for the low-spin ferric species in solution, addition of 1-400 equiv acetic acid has no effect on the decay rate of 2 (0.011(1) s⁻¹ in CH₃CN at 25 °C; see Table S1), suggesting that acetic acid does not interact with the Fe^{III}-OOH species. However, given that the addition of acetic acid eliminates the signals corresponding to the S = 1/2 Fe^{III}-OH species and increases the amount of S = 1/2 Fe^{III}-OOH species (2) formed (Figure S1), we propose that the role of acetic acid is to provide the weakly acidic medium needed to protonate the S = 1/2 Fe^{III}-OH species, converting it into the S = 5/2Fe^{III}-OH₂ species (Scheme 2), by analogy to the closely

Scheme 2. Proposed Role of Acetic Acid in the Formation of



related [(N4Py)Fe^{III}(OH₂)]³⁺ complex described by Browne and co-workers.⁶¹ In this process, the kinetically more inert low-spin Fe^{III}-OH species is replaced by the kinetically more labile high-spin Fe^{III}-OH₂ species that then reacts rapidly with H₂O₂ to achieve the higher steady-state concentration of 2 observed (Figure 1). The corresponding Fe^{III}-O-Fe^{III} species may also be present in the reaction solutions and be involved in these acid-base transformations.

Formation and Characterization of the Intramolecular Phenolate Species Fe^{III}(OAr) (3). Interestingly, when 2 generated with H₂O₂/HOAc reaches its maximum concentration at 25 °C, the addition of 1 equiv of HOTf (p K_a = 2.6 in CH₃CN) with respect to 1 results in the decay of 2 within a second (Figure 1a, dashed blue trace), concomitant with formation of 3, which reaches maximum formation in \sim 300 s (Figure 1). The latter has an intense broad absorption feature spanning from 500 to 1000 nm with a λ_{max} at 680 nm and can be identified as the intramolecular phenolate product 3. This is a result of ortho-hydroxylation of the pendant benzyl ring on the BnTPEN ligand, which converts the ligand into a hexadentate ligand with 5 neutral N donors and 1 anionic O donor. Coordination of the nascent hexadentate ligand to the iron(III) center gives rise to the phenolate-to-iron(III) chargetransfer band associated with 3 (λ_{max} = 680 nm), which is significantly red-shifted relative to that observed for the (μ oxo)diferric complex reported by Feringa and supported by the pentadentate ligand 2-(((di(pyridin-2-yl)methyl)(pyridin-2ylmethyl)amino)methyl)phenolate) with $\lambda_{\text{max}} \sim 540$ nm. ^{62,63} This red shift reflects the higher Lewis acidity of the Fe^{III} center of 3 due to the absence of the highly basic μ -oxo bridge found in the Feringa complex. The rate of formation of 3 and its maximum yield are found to be approximately linearly dependent on the concentration of 1 (Figure S3, left panel), indicating that the hydroxylation reaction is unimolecular in nature. Doubling the amount of HOAc or H2O2 added does not significantly affect the formation rate of 3, but doubling the amount of HOTf added clearly has a deleterious effect on the formation of 3 (Figure S3, right panel).

Given the constraints of the ligand framework, intramolecular hydroxylation at the *ortho*-position of the pendant benzyl ring is the most likely outcome for attack by an iron—oxo species generated at the active site. This conclusion is supported by electrospray ionization (ESI) mass spectrometry (Figure 3 and Figure S4), which shows a molecular ion at m/z 643.0 and an isotope distribution pattern consistent with its formulation as $[(BnTPEN)Fe^{III} + OTf + O - H]^+$. We did not find ions that would support the presence of the corresponding oxo-bridged dimer in solution.

Furthermore, its resonance Raman spectrum is typical of iron(III) centers with an ortho-substituted phenolate ligand (Figure 3 and Figure S5), 63-66 which exhibit a feature around 600 cm⁻¹ that is associated with an Fe-OAr mode and vibrations in the 1100-1600 cm⁻¹ region that correspond to phenolate ring deformation modes. 66 This spectrum exhibits more phenolate ring deformations than found for Fe^{III}-OPh complexes due to the loss of 2-fold symmetry upon orthosubstitution of the phenolate ligand, as observed for [Fe^{III}(EDDHA)] (H₄EDDHA = ethylenediamine-di(2-hydroxyphenylacetic acid)).67 The molar absorptivity of [Fe^{III}(EDDHA)]⁻, which has two phenolates bound to the iron(III) center, is 4800 M⁻¹ cm⁻¹,⁶⁸ about twice the number found for $[Fe^{III}(o,p-EDDHA)]^ (H_4-o,p-EDDHA = ethyl$ enediamine-N-(o-hydroxyphenylacetic)-N'-(p-hydroxyphenylacetic) acid) (2130 M⁻¹ cm⁻¹), where there is only one iron(III) phenolate moiety.⁶⁹ Based on the molar absorptivity coefficients associated with a number of iron(III) orthophenolate compounds, we estimate the molar absorptivity coefficient of the 680 nm chromophore of 3 to be approximately 2000 M⁻¹ cm⁻¹. Although intramolecular aromatic hydroxylation has been demonstrated for related nonheme iron complexes, ^{70–75} this report is, to the best of our knowledge, the first time that intramolecular aromatic hydroxylation has been demonstrated for 1.

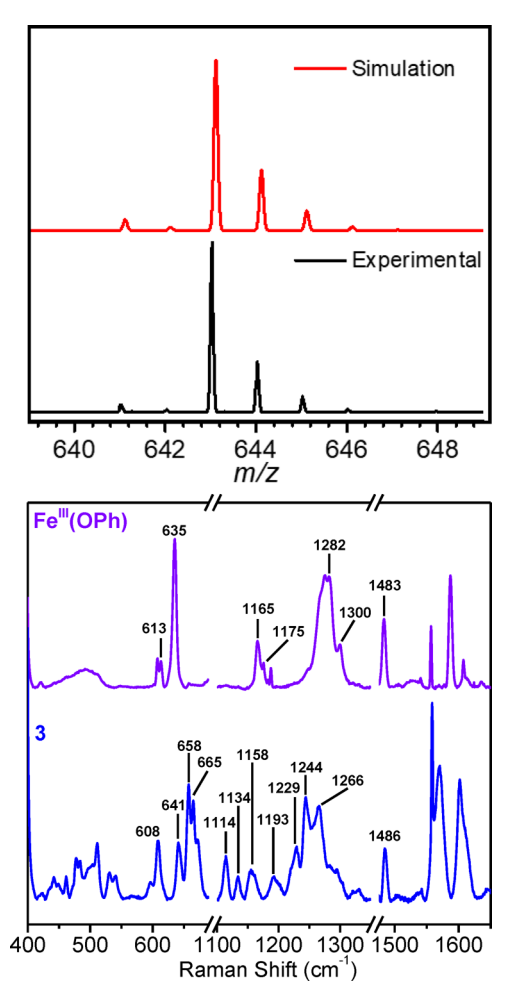


Figure 3. (Top) Expanded molecular ion region of the ESI-MS spectrum of the intramolecular phenolate product 3. See Figure S4 for the full mass spectrum of this species. (Bottom) Comparison of resonance Raman spectra of the intramolecular phenolate product 3 and the intermolecular phenolate product [(BnTPEN)Fe^{III}(OPh)]²⁺ formed in the presence of benzene. Resonance Raman spectra were obtained in CH₃CN at 77 K with 561 nm laser excitation. Reaction conditions: for 3: 1 mM 1 for ESI-MS or 2 mM 1 for resonance Raman, 10 equiv of HOAc, 1 equiv of HOTf in CH₃CN at room temperature. Fe^{III}(OPh) is generated in the same fashion at 1 mM 1 and 100 equiv of benzene in solution. See Figure S5 for the full spectra.

The effects of other acid additives with pK_a values ranging from 0.2 to 23.5 in CH₃CN have been further investigated. These results reveal that the acids studied can be subdivided into two subsets based on the yield of the intramolecular phenolate product formed (Figure S6 and Table S2). The introduction of $HOTs \cdot H_2O$ (pK_a = 8.45 in CH₃CN) or stronger acids generates 3 in high yields ($A_{680} \sim 1$ derived from a solution of 1 mM 1) with no observed accumulation of 2, whereas the addition of HNO₃ (p $K_a = 8.8$ in CH₃CN) or weaker acids leads to much lower yields of 3 ($A_{680} = \sim 0.1$). In the latter cases, the initial accumulation of 2 is also observed in the presence of $Cl_2CHCOOH$ (p $K_a = 13.2$) or weaker acids. The fact that 2 does not accumulate in the presence of strong acids is consistent with the high reactivity observed between 2 and HOTf (Figure 1), suggesting that the strong acid activates the initially formed but unobserved Fe^{III}-OOH species to facilitate the formation of a potent oxidant capable of electrophilic aromatic substitution (EAS) of the pendant phenyl group.

Effect of Acid pK_a on Cyclohexane and Benzene Hydroxylation at Room Temperature. The highly oxidizing nature of this new oxidant generated in the presence of strong acids is demonstrated by the facile intermolecular oxidation of cyclohexane, a hydrocarbon substrate with very strong C-H bonds (BDE = 99.5 kcal mol^{-1})⁷⁶ (Figure 4 and

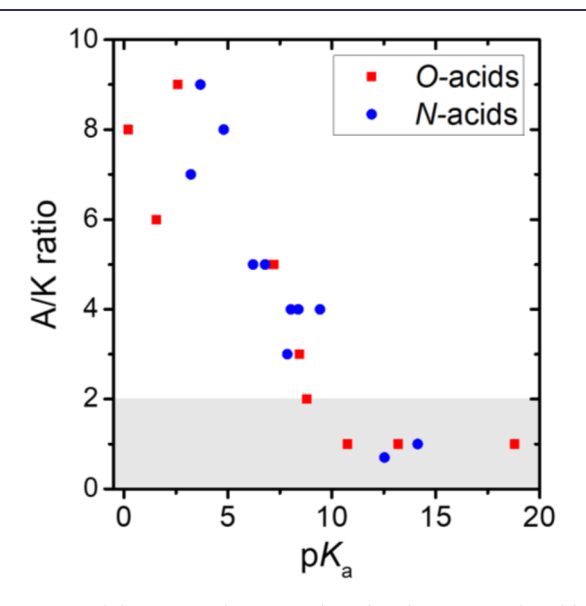


Figure 4. Cyclohexane oxidation product distributions catalyzed by 1 in the presence of various acids. See the reaction conditions under Table 1.

Table 1). The use of HOTf (p K_3 = 2.6 in CH₃CN) results in the catalytic formation of cyclohexanol (3.6 turnovers from 10 equiv 90% H₂O₂) with an alcohol-to-ketone (A/K) ratio of 9. The high A/K ratio argues for a mechanism involving the generation of a highly reactive Fe^V=O oxidant that performs HAT on the substrate C-H bond directly followed by rapid rebound of the nascent alkyl radical with the incipient Fe^{IV}-OH moiety.⁷⁷ Acids with comparable pK_a values, such as HBF₄·Et₂O (0.2) and HClO₄ (1.57), give outcomes with similarly high A/K ratios (Figure 4 and Table 1). The observed high A/K ratio is not significantly affected by the presence of O₂ as shown in the case of HOTf addition (Figure S7), indicating that the alkyl radicals if formed must rebound too quickly to be intercepted by O2. Under these conditions, the reaction mixtures turn light blue during the course of the reactions, suggesting that intramolecular aromatic hydroxylation occurs to some extent. On the other hand, the addition of weaker acids having p K_a 's > 8.5 affords smaller amounts of cyclohexanol and cyclohexanone but in comparable yields, so the A/K ratios approach 1; such an outcome is typically associated with the formation of long-lived carbon-centered radicals. Therefore, as the p K_a decreases from >8.5 to <2, a transition from low to high A/K selectivity is observed that generally correlates with the pK_a of the added acid (Figure 4).

The O-based acids in this study can also be replaced by Nbased acids such as pyridinium and anilinium salts, which exert similar effects as the O-based acids with comparable pK_a values (Table 1), indicating that the observed reactivity depends mainly on the acidity of protons added. This pK_a -dependent behavior in cyclohexane oxidation reactivity also coincides with

Table 1. Cyclohexane Oxidation by 1 with H₂O₂ in the Presence of Acids at Room Temperature

$$\begin{array}{c|c} & 10 \text{ eq HOAc} & \text{OH} & \text{O} \\ \hline 10 \text{ eq 90\%H}_2\text{O}_2 & & & \\ \hline 1 \text{ eq acid} & & & \\ \hline 1 & \text{CH}_3\text{CN, RT, 2h} & & & \\ \hline \end{array} + \begin{array}{c} \text{OH} & \text{O} \\ & \text{He} \\ & \text{OH} \\ & \text{CH}_3\text{CN, RT, 2h} \\ \end{array}$$

| pK_a^b | alcohol (TON) | ketone (TON) | A/K ratio |
|----------|---|---|--|
| 0.2 | 3.2(2) | 0.4(1) | 8 |
| 1.57 | 3.2(1) | 0.5(1) | 6 |
| 2.6 | 3.6(1) | 0.4(1) | 9 |
| 3.22 | 3.3(3) | 0.5(1) | 7 |
| 3.68 | 3.5(1) | 0.4(1) | 9 |
| 4.8 | 3.3(1) | 0.4(1) | 8 |
| 6.21 | 2.9(1) | 0.6(1) | 5 |
| 6.79 | 4.2(2) | 0.9(1) | 5 |
| 7.2 | 3.8(1) | 0.8(1) | 5 |
| 7.86 | 2.3(2) | 0.8(1) | 3 |
| 8.03 | 3.3(1) | 0.8(1) | 4 |
| 8.39 | 2.9(5) | 0.7(2) | 4 |
| 8.45 | 2.1(1) | 0.7(1) | 3 |
| 8.8 | 1.6(1) | 1.0(3) | 2 |
| 9.43 | 2.2(1) | 0.6(1) | 4 |
| 10.75 | 1.5(2) | 1.5(1) | 1 |
| 12.53 | 2.4(3) | 3.3(4) | 0.7 |
| 13.2 | 1.6(1) | 1.4(1) | 1 |
| 14.13 | 1.4(2) | 1.4(1) | 1 |
| 18.8 | 1.5(2) | 1.3(1) | 1 |
| 23.5 | 1.5(1) | 1.2(1) | 1 |
| | 0.7(2) | 1.1(1) | 0.7 |
| | 1.57 2.6 3.22 3.68 4.8 6.21 6.79 7.2 7.86 8.03 8.39 8.45 8.8 9.43 10.75 12.53 13.2 14.13 | 0.2 3.2(2) 1.57 3.2(1) 2.6 3.6(1) 3.22 3.3(3) 3.68 3.5(1) 4.8 3.3(1) 6.21 2.9(1) 6.79 4.2(2) 7.2 3.8(1) 7.86 2.3(2) 8.03 3.3(1) 8.39 2.9(5) 8.45 2.1(1) 8.8 1.6(1) 9.43 2.2(1) 10.75 1.5(2) 12.53 2.4(3) 13.2 1.6(1) 14.13 1.4(2) 18.8 1.5(2) 23.5 1.5(1) | 0.2 3.2(2) 0.4(1) 1.57 3.2(1) 0.5(1) 2.6 3.6(1) 0.4(1) 3.22 3.3(3) 0.5(1) 3.68 3.5(1) 0.4(1) 4.8 3.3(1) 0.4(1) 6.21 2.9(1) 0.6(1) 6.79 4.2(2) 0.9(1) 7.2 3.8(1) 0.8(1) 7.86 2.3(2) 0.8(1) 8.03 3.3(1) 0.8(1) 8.39 2.9(5) 0.7(2) 8.45 2.1(1) 0.7(1) 8.8 1.6(1) 1.0(3) 9.43 2.2(1) 0.6(1) 10.75 1.5(2) 1.5(1) 12.53 2.4(3) 3.3(4) 13.2 1.6(1) 1.4(1) 14.13 1.4(2) 1.4(1) 18.8 1.5(2) 1.3(1) 23.5 1.5(1) 1.2(1) |

^aAn = anilinium. BF₄ is the counteranion of all pyridinium and anilinium salts. ${}^{b}pK_{a}$ values obtained from refs 79 and 80. TON = turnover number with respect to the catalyst. A/K ratio calculated by dividing cyclohexanol TON by cyclohexanone TON. The intramolecular phenolate product 3 is not quantified for catalysis reactions. Maximum A_{680} values representing the yields of 3 obtained without cyclohexane as the competing substrate are listed in Table S2. Reaction conditions: 1 mM 1, 10 equiv of HOAc, 1 equiv of various acids, 10 equiv of 90% H₂O₂, and 1000 equiv of cyclohexane in CH₃CN at room temperature. The solutions were prepared in a N₂ glovebox except for acid and H₂O₂ stock solutions, which together account for 2% of the total volume of the reaction mixture. The results are the average of at least two trials.

the observation of significant intramolecular aromatic hydroxylation reactivity for acids with pK_a values below 8.5 (Figure S6), indicating that this putative metal-based oxidant is capable of cleaving strong C-H bonds as well as electrophilic aromatic hydroxylation.

All of the experiments discussed above have been carried out with dry reagents and solvent, with the only water introduced coming from the 10 equiv of 90% H₂O₂ added, which contains about 2 equiv of H2O. With this small amount of water present, the A/K ratio from cyclohexane oxidation in the presence of HOAc/HOTf is not significantly affected by the presence of O₂ (Figure S7). However, increasing the amount of water present in the reaction mixture lowers the A/K selectivity of 1 in cyclohexane oxidation. For example, the A/K ratio of 8 obtained from a reaction mixture containing HOAc/ HOTf and 10 equiv of 90% H₂O₂ reduces to 5 when 100 equiv water is added (Figure S8), which approximates the amount of water present in 10 equiv of 30% H_2O_2 (88 equiv H_2O). Increasing the amount of water present further decreases the A/K ratio such that it becomes unity with 1000 equiv of H_2O ,

showing that the nature of the oxidant is altered dramatically in the presence of larger amounts of water. The deactivating effect of water observed in the case of 1 may arise from its leveling effect, which attenuates the electrophilicity of the proton and favors O-O bond homolysis of 2 over its

The generation of an Fe^V=O oxidant in the presence of strong acids is further corroborated by labeling studies with H₂¹⁸O₂ or H₂¹⁸O (Table 2). Cyclohexane hydroxylation

Table 2. Effect of Added Water on the A/K Product Ratios and the % ¹⁸O-Incorporation into the Cyclohexanol Product

| | A /T7 | equiv of | 11 180 | 11 180 | c |
|---|-------|------------------------|---------------|-------------|--------------|
| | A/K | H ₂ O added | $H_2^{18}O_2$ | $H_2^{18}O$ | ref |
| 1 + HOTf + HOAc under Ar | 5 | 200 | 93(1) | 6(1) | this work |
| 1 + HOTf + HOAc | 9 | 0 ^a | | | |
| 1 + HOTf + HOAc | 5 | 100 | | 1.4(2) | |
| | 4 | 200 | 69(4) | 4.2(1) | |
| | 3 | 400 | | 6.9(2) | |
| 1 + HOAc | 1 | 200 | 10(1) | 0.9(1) | |
| $Fe^{II}(CH_3CN)_2(OTf)_2$ | 2 | 200 | | 0.5(3) | this |
| $Fe^{II}(CH_3CN)_2(OTf)_2 + HOTf + HOAc$ | 1 | 200 | | 0.6(1) | work |
| Fe(N4) (CH ₃ CN) ₂ (ClO ₄) ₂ ^b | | | | | |
| N4 = TPA | 5 | 1000 | 70 | 27 | 45 |
| $N4 = 5-Me_3TPA$ | 9 | 1000 | 69 | 38 | 45 |
| | | 400 | | 30 | 45 |
| N4 = BPMEN | 8 | 1000 | 84 | 18 | 81 |
| $N4 = {}^{Me2}PyTACN$ | 12 | 1000 | 47 | 42 | 47 |

^aThe only water present is the 2 equiv of H₂¹⁶O in the 10 equiv of 90% H₂¹⁶O₂ added. This entry has been included to show the effect of added water in the reaction. Reaction conditions are listed under Table 1. b For these reactions, either 10 equiv of $30\%^{45,81}$ or $35\%^{47}$ of H₂O₂ was used for H₂¹⁸O labeling studies. About 100 equiv of H₂¹⁶O was present in each of these reaction mixtures. BPMEN = N_iN' bis(pyridylmethyl)ethylenediamine. Reaction conditions: 1 mM Fe complex or salt, with or without 1 equiv of HOTf and/or 10 equiv of HOAc, 10 equiv of 10% H₂¹⁸O₂ (90% ¹⁸O enriched in H₂¹⁶O, contains about 200 equiv $H_2^{16}O$ when adding 10 equiv) or 10 equiv of 90% $H_2^{16}O_2$ along with 200 equiv of $H_2^{18}O$ and 1000 equiv of cyclohexane in CH₃CN at room temperature in air.

performed under an inert atmosphere with 10% H₂¹⁸O₂ (90% ¹⁸O-enriched in H₂¹⁶O, a 10 equiv aliquot of which would contain 10 equiv of $H_2^{18}O_2$ and ~200 equiv of $H_2^{16}O$), 1 equiv of HOTf, and 10 equiv of HOAc affords cyclohexanol products with 93(1)% and 6(1)% ¹⁸O-incorporation, respectively, from H₂¹⁸O₂ and H₂¹⁸O, together accounting for 100% of the oxygen atom found in the alcohol product. Under air, the reaction affords cyclohexanol with 69% ¹⁸O-incorporation from $H_2^{18}O_2$ and 4% ^{18}O -incorporation from $H_2^{18}O$, the remaining 27% product presumably incorporating its O-atom from O2. When the 1 equiv HOTf additive is excluded, only 10% ¹⁸O-incorporation from H₂¹⁸O₂ into cyclohexanol is observed, with negligible incorporation of $^{18}\mathrm{O}$ from $\mathrm{H_2}^{18}\mathrm{O}$ in the complementary experiment with 10 equiv of 90% H₂¹⁶O₂ (containing 2 equiv of H₂¹⁶O) and 200 equiv of H₂¹⁸O. The high degree of ¹⁸O-labeling from H₂ ¹⁸O₂ in the alcohol product in the presence of HOTf is consistent with a C-H bond hydroxylation mechanism involving HAT by a metal-oxo species followed by rapid rebound.⁷⁷ However, the larger amount of water present in the 10% H₂¹⁸O₂ solution

diminishes the electrophilicity of the HOTf proton and opens the door for a competing pathway that generates a longer lived alkyl radical that can be intercepted by O2, hence decreasing the A/K ratio.

This deleterious effect of added water in the case of 1 is quite different from the observed positive effect of added water in Fe(TPA)-catalyzed oxidations. 45,46,50 For the latter, addition of 400 equiv of water accelerates the rate of heterolytic O-O bond cleavage by as much as 7-fold⁵⁰ and results in a 30% incorporation of oxygen label from water into the cyclohexanol product. 45 In significant contrast, the presence of just 50 equiv of water cuts the rate of HOTf (1 equiv)-assisted heterolytic O-O bond cleavage of 2 at -40 °C from $k_{obs} = 0.9(1) \text{ s}^{-1}$ without added H₂O to 0.015(1) s⁻¹ with 50 equiv of H₂O, for a 60-fold difference (Figure S9, detailed kinetics discussions of the decay of 2 in the following section). Also, as shown in Table 2, only a small fraction of the alcohol product from 1catalyzed cyclohexane hydroxylation incorporates the ¹⁸O label from the added H₂¹⁸O. These results suggest the participation of a minor pathway related to the water-assisted mechanism established for Fe(TPA)-catalyzed hydrocarbon oxidations to generate an Fe^V(O)(OH) oxidant. Such a pathway would likely require dissociation of a pyridyl arm, as previously documented for complexes of TPEN and related ligands, 82 in order to open up a coordination site for the water to bind. However, given the small extent of ¹⁸O incorporation from H₂¹⁸O, such a pathway would likely not be the major pathway for cyclohexane hydroxylation by 1.

We have also investigated the use of benzene as an intermolecular substrate for EAS to further probe the nature of this oxidant (Figure 5). About 5 TON of phenol product is

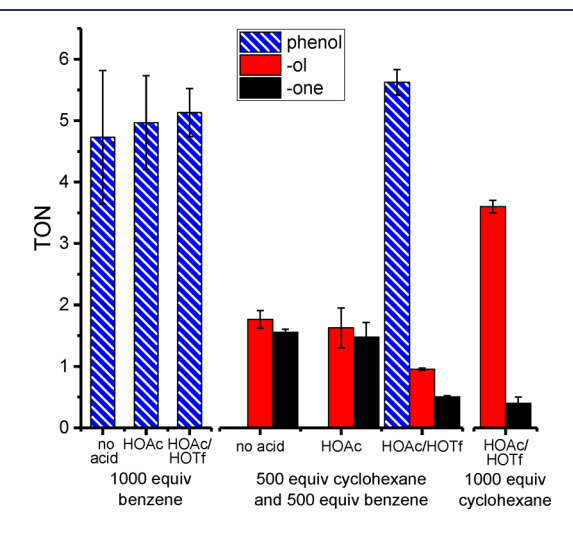


Figure 5. Benzene hydroxylation by 1/H2O2 under different conditions and in competition with cyclohexane. Reaction conditions: 1 mM 1 and 10 equiv of 90% H2O2 with or without 10 equiv of HOAc and 1 equiv of HOTf in CH₃CN at room temperature in air. A small amount of phenol product can be observed in the presence of 500 equiv of cyclohexane and 1000 equiv of benzene in the absence of any acid or upon addition of HOAc only; see Table S5.

obtained in the presence of HOAc/HOTf, consistent with the intramolecular EAS reactivity exhibited by the complex. Competition experiments between benzene and cyclohexane at a 1:1 molar ratio shows a 5:1 preference for hydroxylation of benzene over cyclohexane. Similar preferences for EAS over HAT have been reported for related systems where Fe^V=O

Table 3. PKIEs for Hydrocarbon Oxidations by 1 and Related Complexes

| reactions at room temperature | benzene | cyclohexane | ref |
|---|------------|--------------|--------|
| | (EAS) | (HAT) | |
| $1 + H_2O_2$ | 1.0 | 1.8 | а |
| 1 + HOAc + H2O2 | 1.2 | 1.9 | а |
| $1 + HOAc + H2O2 + HOTs \cdot H2O$ | 0.9 | 2.1 | а |
| $1 + HOAc + H_2O_2 + HOTf$ | 0.9 | 2.3 | а |
| $Fe^{II}(BPMEN)(CH3CN)2(ClO4)2 + H2O2$ | 0.8 | 3.2 | 45, 90 |
| $[Fe^{II}(Py_2NHC_2)(CH_3CN)_2](PF_6)_2^b + H_2O_2$ | 0.9 | | 91 |
| $[(PDP^*)Fe^{III}(\mu-OH)_2Fe^{III}(PDP^*)](OTf)_4 + CH_3CO_3H/H_2O_2 + HOAc$ | 0.9 | | 93 |
| $[(MeTPEN)Fe^{II}(Cl)]Cl + H2O2 + ArSHd$ | 1.2 | | 58 |
| $Fe(CH_3CN)_2(OTf)_2 + HOAc + H_2O_2 + HOTf$ | 1.2 | 2.2 | a |
| $(FePctBu_4)_2N + H_2O_2$ | 1.2-1.3 | | 94 |
| $[(BnTPEN)Fe^{IV}(O)]^{2+}$ | anthracene | ethylbenzene | 89, 95 |
| | 0.86 | 50 | |

"This work. Reactions conditions for this work: 1 mM 1, 10 equiv of HOAc, 10 equiv of 90% H_2O_2 , 1 equiv of HOTf, 500 equiv of unlabeled and 500 equiv of perdeuterated benzene or cyclohexane in CH_3CN at room temperature in air. $^bPy_2NHC_2 = bis(o-imidazol-2-ylidenepyridine)$ -methane. $^cN_1N'$ -Bis(3,5-dimethyl-4-methoxypyridyl-2-methyl)-($S_1S_1S_2$ -2, S_2S_2 -bipyrrolidine. dArSH serves as a radical scavenger and is added to improve catalytic conversion. S_1S_2 $^cPctBu_4 = tetrakis(tert-butyl)$ phthalocyanine dianion.

species have been proposed to be the active oxidant. S6,85 Reactions using a 1:1 mixture of benzene and perdeuterated benzene (Table 3) reveal a product kinetic isotope effect (PKIE) of 0.9, demonstrating preferential oxidation of the deuterated isotopomer. Such an inverse PKIE is consistent with electrophilic attack of the aromatic ring by an Fe^V=O species, where the PKIE would originate from a change in hybridization of the hydroxylated carbon atom from sp^2 to sp^3 during the formation of a σ -complex. S8,86-93

Comparable amounts of phenol products, about 5 TON, are also found in the oxidation of benzene by 1 with no acid added or with only HOAc introduced (Figure 5). Even when 1 is replaced with an iron salt, Fe^{II}(CH₃CN)₂(OTf)₂, to induce Fenton-type reactions, about 4 TON of phenol can still be obtained (Table S3). These observations show that benzene hydroxylation to phenol can be readily carried out by hydroxyl radicals. ¹⁸O-labeling studies suggest that the majority of oxygen atoms found in the phenol product originates primarily from H₂O₂ regardless of whether the reaction is performed in the presence of strong acids (Table S4). However, in sharp contrast to the reactions in the presence of strong acids, competition experiments between benzene and cyclohexane with no acid or HOAc result in the preferential oxidation of cyclohexane, with A/K product ratios similar to that obtained in the absence of benzene (Figure 5 and Table 1). A similar preference toward cyclohexane oxidation is observed for Fe^{II}(CH₃CN)₂(OTf)₂ (Table S3). Furthermore, PKIE values of 1.0-1.2 are observed for benzene oxidation with Fe^{II}(CH₃CN)₂(OTf)₂ or with 1 in the absence of acid or in the presence of HOAc, resembling that obtained for benzene hydroxylation by Fe(MeTPEN) and H₂O₂ reported by Banse and co-workers, where the hydroxyl radicals are proposed to be the active oxidant. 40,58 Taken together, the drastic differences in HAT/EAS reactivity and PKIE clearly distinguish the Fe^V=O oxidant generated in the presence of strong acids and radicals generated in the presence of no acid or weak acids.

Kinetic Studies of the Reaction of 2 with Acids at -40 °C. To systematically assess the effect of acids with a range of p K_a values on the decay of the Fe^{III}-OOH species, 2 was first generated at room temperature with 10 equiv of HOAc and 10 equiv of 90% H_2O_2 for 1 min to achieve a yield of \sim 50% and then cooled to -40 °C for kinetic studies. Under these

conditions, the Fe^{III}-OOH species formed eventually achieves a maximum absorbance at 525 nm corresponding to ~70% conversion (Figure 6). The benefits of using the H₂O₂/HOAc combination to generate the intermediate are 3-fold: (1) it circumvents the need for a large excess of H2O2 typically required to generate this Fe^{III}-OOH species, as only 10 equiv of H₂O₂ and 10 equiv of HOAc are needed to generate the Fe^{III}-OOH species in more than double the yield obtained when 100 equiv of H_2O_2 is used alone (Figure 1); (2) the EPR spectrum of the $H_2O_2/HOAc$ reaction mixture shows the S =1/2 Fe^{III}-OOH species to be the only EPR-active iron species in solution, whereas significant amounts of signals originating from ferric byproducts such as the Fe^{III}-OH species are also observed when using H₂O₂ alone (Figure S1); (3) HOAc is the weakest acid in our study (p $K_3 = 23.5$ in CH₃CN) and likely does not directly interact with the Fe^{III}-OOH species, as the decay rate of 2 is independent of HOAc concentration (Table S1), thereby allowing it to be used as a baseline for reactivity studies with other acids. Unlike experiments at room temperature where the Fe^{III}-OOH species forms rapidly, 2 does not regenerate appreciably on the time scale of its reactions with strong acids at -40 °C, which only take seconds. Therefore, its reactions with the strong acids can be treated as stoichiometric transformations between the acid and 2 at its steady-state concentration.

The solution of 2 formed as described above is quite stable at -40 °C. It persists for 1 h with hardly any change in absorbance and decays completely over the course of 16 h. A $k_{\rm decay}$ value of 2.4 \times 10⁻⁵ s⁻¹ at -40 °C can be extrapolated from an Eyring plot based on rate data obtained at higher temperatures (Figure S10). The addition of strong acids to 2 results in the immediate decay of 2, dramatically decreasing the lifetime of 2 by 4 orders of magnitude, from hours to seconds. Simultaneously, 3 is formed with an apparent isosbestic point at 625 nm (Figure 6). Cyclohexane and benzene both can intercept the active oxidant, as their introduction results in a decrease in yield of 3 in the case of cyclohexane or the formation of the Fe^{III}-OPh chromophore in the case of benzene (Figures S11 and S12). Excess H₂O₂ in solution may also serve as a substrate, as the introduction of additional H_2O_2 leads to a decrease in the yield of 3 (Figure S13).

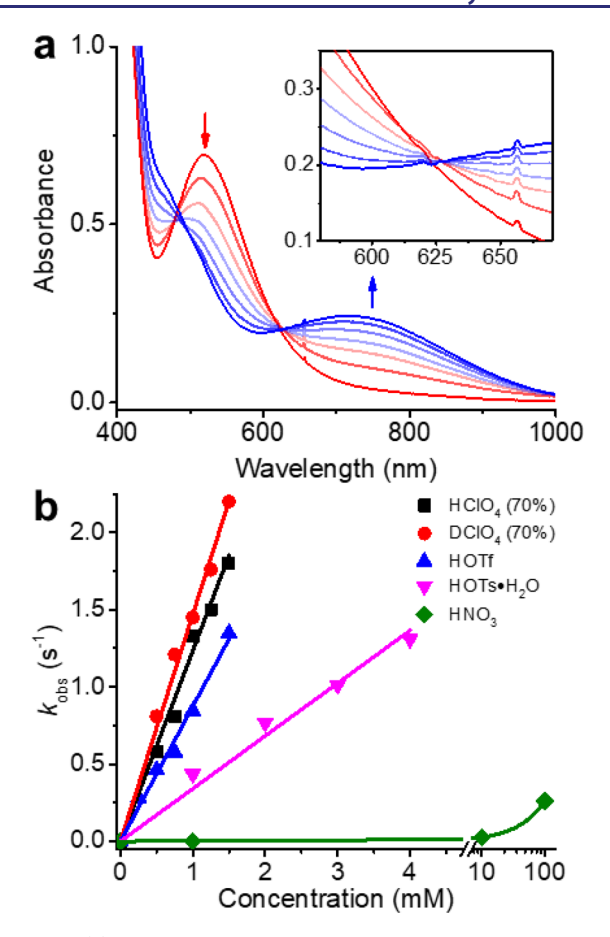


Figure 6. (a) Representative spectra obtained from the reaction of 2 with 1 equiv of HOTf at -40 °C taken over the course of 5 s. (b) First-order decay rates of 2 plotted as a function of acid and its concentration. Reaction conditions: acid added to a solution of 2 at -40 °C, which was first generated with 1 mM 1, 10 equiv of HOAc, and 10 equiv of 90% $\rm H_2O_2$ in CH₃CN at room temperature and then cooled to -40 °C. Errors for the second-order rate constants obtained for the slopes of the linear plots were estimated to be less than 10%.

Intermediate 2 decays exponentially, and the first-order rate constants derived therefrom increase as a function of acid concentration to afford second-order rate constants from the slopes of the linear plots (Figure 6). The decay rates of 2 also depend on the pK_a of the added acid. Thus, the addition of HClO₄ (70%) to a solution of 2 gives rise to an Fe^{III}-OOH decay rate of 1300 M⁻¹ s⁻¹, the fastest reported thus far (Table 4, Figure 7), followed by HOTf (870 M⁻¹ s⁻¹) and HOTs. H_2O (340 M^{-1} s⁻¹). In the latter case, the addition of HOTs· H_2O to a solution of 2 at -40 °C results in the formation of a different chromophore at 650 nm, which likely derives from hydroxylation of HOTs. These three k_2 values differ by only a factor of 4 despite having pK_a's in CH₃CN that range from 1.6 to 8.5. Surprisingly, HNO₃ with a pK_a of 8.8 in CH₃CN reacts with 2 with a second-order rate constant of 2.6 M⁻¹ s⁻¹, which is 2 orders of magnitude slower than that for HOTs·H₂O, even though the two acids differ by only ~ 0.3 of a p K_a unit in CH₃CN. At the same time, the A/K ratio observed for cyclohexane hydroxylation for this entire series of acids decreases from 9 to 1 upon replacing a strong acid with an acid having pK_a in CH₃CN of more than 8.5 (Table 1), and the amount of 3 that is formed also drops significantly (Figure S6, Table S2). These results suggest a change in mechanism in which the addition of an acid as strong or stronger than HOTs.

Table 4. Decay of 2 in the Presence of Various Acids at -40 $^{\circ}$ C^a

| acid | pK_a | $k_2 (M^{-1} s^{-1})$ |
|---|--------|-----------------------|
| HClO ₄ (70% in H ₂ O) | 1.57 | 1300 |
| DClO ₄ (68% in D ₂ O) | | 1500 |
| HOTf | 2.6 | 870 |
| $HOTs \cdot H_2O$ | 8.45 | 340 |
| HNO ₂ | 8.8 | 2.6 |

"Second-order rate constants were extracted from Figure 6b. Rates obtained for 3 formation at 825 nm and 2 decay at 580 nm were almost identical (Figure S14) and thus were treated as equivalent information. Rates for reactions of 2 with HNO₃ were obtained by monitoring the decay of 2 at 580 nm. Rates for reactions of 2 with HOTs·H₂O were obtained by monitoring 650 nm chromophore formation at 825 nm.

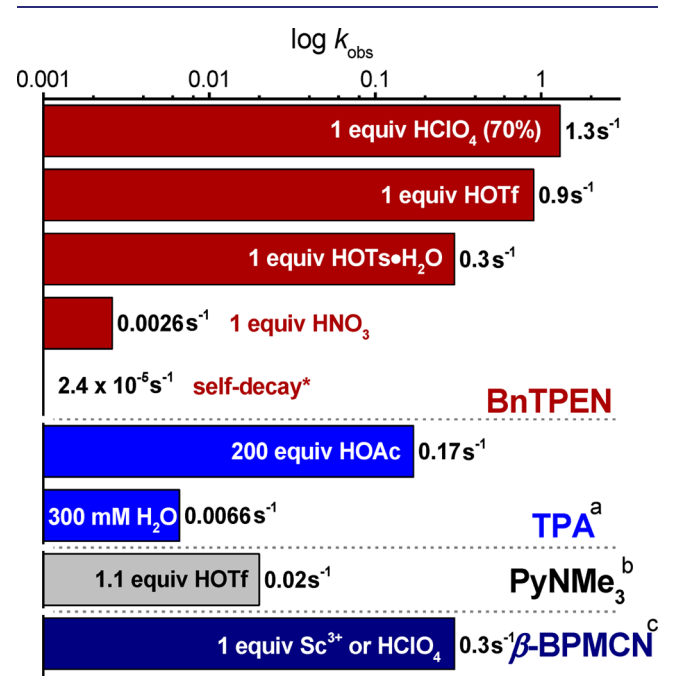


Figure 7. First-order decay rates for (L)Fe^{III}-OOH species at -40 °C. *The self-decay rate of 2 at -40 °C was estimated from an extrapolation from the Eyring plot for the decay of 2 in the presence of HOAc measured at higher temperatures (Figure S10). (a) References 50 and 96. (b) Reference 55. (c) Reference 56.

 H_2O favors a proton-assisted O–O bond heterolysis of the Fe $^{\rm III}$ –OOH intermediate 2, which is in competition with the O–O bond homolysis pathway inherent to 2. A similar pH-dependent switch at pH \sim 9 in the outcome of O–O bond cleavage has been reported by van Eldik and co-workers in the reaction of a water-soluble porphyrin with $H_2O_2^{\ 24}$

We have also investigated whether a higher concentration of a weak acid such as 100 equiv of HNO₃ could facilitate the decay of 2 and give rise to the Fe^V=O oxidant. However, the decay rate of 2 under these conditions remains considerably slower than with addition of 1 equiv of HOTs·H₂O (Figure 6). The reactivity of 2 toward cyclohexane also does not change significantly upon addition of 100 equiv of HNO₃, suggesting no change in the reaction mechanism despite the higher concentration of this weak acid (Figure S15). On the other hand, adding an excess of strong acid is found to be detrimental to the reaction, with the total yield of cyclohexane-derived products dropping to only 2 TON and the

A/K ratio approaching unity (Figure S15). Some ligand dissociation from the iron complex could occur under such conditions, allowing for a Fenton-type reaction to dominate instead.

The use of DClO₄ in place of HClO₄ results in a 10% faster rate of decay or an inverse H/D isotope effect of 0.9 (Table 4). This effect differs from the solvent KIE (KSIE) values obtained for reactions where the proton delivered to the peroxo species likely originates from a weak acid, such as a water molecule in the formation of Cpd I from Cpd 0 in horseradish peroxidase (1.7),⁹⁷ the conversion of the diferric–peroxo intermediate of soluble methane monooxygenase (sMMO) to the diiron(IV) intermediate Q (1.4 and 1.8), ^{98,99} or the water-assisted O–O heterolysis of the (TPA)Fe^{III}–OOH species (2.5). ⁵⁰ In these latter examples, the KSIE observed likely originates from the cleavage of the water O-H/(D) bond prior to or concomitant with O-O bond cleavage of the hydroperoxo moiety. In our reactions with perchloric acid, the slightly faster rate obtained with DClO₄ may be the result of an equilibrium isotope effect, favoring the formation of an Fe^{III}-OOH···D adduct over an Fe^{III}-OOH···H adduct, as deuterium can form a stronger bond with oxygen than protium. Taken together, the data strongly favors a mechanism where a proton is directly involved in O-O bond heterolysis of the Fe¹III-OOH species.

Eyring analysis has been carried out to gain further insight into the rate determining O–O bond cleavage step (Table 5 and Figure S10). In the presence of HOAc, the decay of 2 has Eyring parameters of $\Delta H^{\ddagger} = 52(2)$ kJ mol⁻¹ and $\Delta S^{\ddagger} = -108(10)$ J K⁻¹·mol⁻¹. These values are very close to those found for the decay of 2 in CH₃OH³⁵ and almost identical to

Table 5. Eyring Activation Parameters for the Decay of (L)Fe $^{\rm III}$ – OOR Complexes

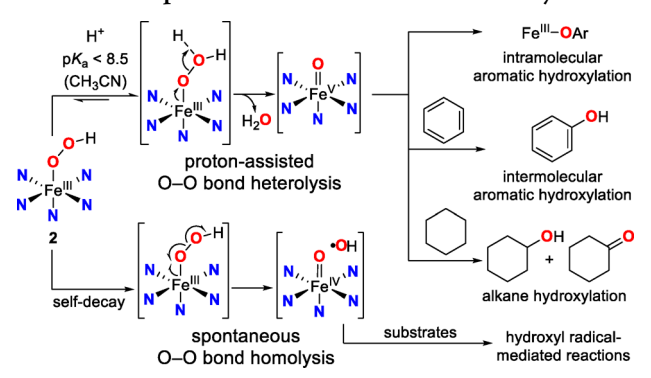
| - | | | | |
|---|---|---------------------------------|---------------------------------------|-----|
| | $\Delta H^{\ddagger} \ (\mathrm{kJ/} \ \mathrm{mol})$ | ΔS^{\ddagger} J/(K·mol) | proposed O-O bond cleavage mode | ref |
| 2 + HOAc + HOTf in CH ₃ CN | 30(2) | -118(20) | heterolysis | а |
| 2 + HOAc in CH ₃ CN | 52(2) | -108(10) | homolysis | а |
| 2 in CH ₃ OH | 53(2) | -72(8) | homolysis | 35 |
| (MeTPEN)Fe ^{III} -OOH in CH ₃ CN | 81 | -1 | homolysis | 58 |
| (N4Py)Fe ^{III} –OOH in acetone/CF ₃ CH ₂ OH | 53(1) | -121(2) | homolysis | 103 |
| (bbpc)Fe ^{III} –OOH in CH ₃ CN | 53(1) | -68(4) | homolysis | 104 |
| (TPA)Fe ^{III} –OO ^t Bu in CH ₃ CN | 52(1) | -74(3) | homolysis | 105 |
| $(TPA)Fe^{III}(\kappa^2-O_2C(CH_3)_2OH)$ in acetone | 54(3) | -35(13) | homolysis | 106 |
| $(TPA)Fe^{III}$ -OOH in CH_3CN | 45(2) | -95(10) | heterolysis | 50 |
| $(PyNMe_3)Fe^{III}$ $-OOH$ in CH_3CN | 44(3) | -138(12) | homolysis | 55 |
| (PyNMe ₃)Fe ^{III} –OOH in CH ₃ CN with 1.1 equiv of HOTf | 46(4) | -79(13) | heterolysis | 55 |
| $(14\text{-TMC})\text{Fe}^{\text{III}}$ $-\text{OOH}$ in acetone/CF ₃ CH ₂ OH | 56(2) | -75(2) | homolysis | 103 |
| (14-TMC)Fe ^{III} –OOH + HClO ₄ in CH ₃ CN | 44(2) | -90(10) | heterolysis | 107 |

^aThis work. bbpc = N,N'-dibenzyl-N,N'-bis(2-pyridylmethyl)-1,2-cyclohexanediamine. 14-TMC = 1,4,8,11-tetramethyl-1,4,8,11-tetraazacyclotetradecane. See Figure S10 for Eyring plots and reaction conditions.

that obtained for (N4Py)Fe^{III}-OOH in CH₃OH, both of which have been proposed to undergo rate-determining homolytic O-O bond scission. The lack of a dramatic change in Eyring parameters upon addition of HOAc further supports our hypothesis that HOAc does not play a significant role in the O-O bond-cleavage step. In stark contrast, the addition of 1 equiv of HOTf to the solution of 2 drastically lowers its ΔH^{\ddagger} by 22 kJ mol⁻¹ to 30(2) kJ mol⁻¹, reflecting the significantly more rapid decay of 2 in the presence of HOTf. This activation enthalpy is the smallest ΔH^{\ddagger} value we have determined for the decay of an Fe^{III}-OOH species and at least 14 kI mol⁻¹ smaller than values associated with Fe^{III}-OOH complexes supported by tetradentate ligands such as TPA, PyNMe₃ and TMC that undergo heterolytic cleavage of the O-O bond, even upon treatment with strong acid (Table 5). Thus, the proton-induced heterolytic O-O bond cleavage of the (BnTPEN)Fe^{III}-OOH intermediate 2 is distinct from the other complexes and more facile, unleashing quite a powerful Fe^V=O oxidant capable of rapidly cleaving strong C-H bonds even at -40 °C.

Mechanistic Insights. We propose that an Fe^V=O species is responsible for the oxidation reactions observed when 2 is treated with strong acids (Scheme 3). Strong acids promote

Scheme 3. Proposed Mechanism for the Reactivity of 2



heterolytic scission of the O-O bond of the Fe^{III}-OOH species, producing an Fe^V=O species that hydroxylates cyclohexane to cyclohexanol and benzene to phenol within seconds at -40 °C, which is unprecedented for 2 and related Fe(N5) complexes. The decay rate of the Fe^{III}-OOH species is linearly correlated with the concentration of the strong acid used and is faster for acids with lower pK, values (Figure 6b and Table 4). An Eyring plot obtained for Fe^{III}-OOH decay in the presence of HOTf shows a dramatic decrease of 22 kJ mol^{$^{-1}$} in ΔH^{\ddagger} relative to the 52 kJ mol^{$^{-1}$} value typical for O–O bond homolysis (Table 5), ^{35,103} suggesting that O–O bond heterolysis is greatly facilitated by strong acids. Taken together, the data strongly support the direct involvement of a proton in the O-O bond cleavage of the Fe^{III}-OOH species by facilitating the departure of the distal OH group by pulling it away as water, thereby promoting the formation of an Fe^V=O species without compromising its electrophilicity.

Prior to the current work, the best supported examples of proton-assisted O–O bond heterolysis of Fe^{III}–OOH species in nonheme model systems occur via what is known as the water-assisted pathway, which is associated with bioinspired nonheme iron catalysts for hydrocarbon oxidations that are supported by tetradentate N4 ligands such as TPA, BPMEN, and Me²PyTACN. ^{50,51,85} In this class of catalysts, an iron-

bound water molecule is conveniently positioned cis to the Fe^{III}-OOH moiety, allowing for hydrogen-bonding interactions between a proton of the cis-bound water to the distal oxygen of the hydroperoxide, thereby forming a fivemembered-ring transition state that facilitates O-O bond heterolysis and the formation of the putative $Fe^{V}(O)(OH)$ oxidant (Scheme 1). Subsequent oxo/hydroxo tautomerism allows the oxygen atom from H2O to be incorporated into the Fe^V=O unit. This mechanistic scenario was conceived 20 years ago for the Fe(BPMEN) catalyst to account for the observed partial ¹⁸O-labeling of hydroxylated products when the reactions were carried out in the presence of H₂¹⁸O⁸¹ and has since been confirmed for other Fe(N4) catalysts like Fe(TPA)⁴⁵ and Fe(Me2PyTACN)⁴⁷ among others. Subsequently, evidence for the Fe^V(O)(OH) oxidant was obtained from mass spectrometry experiments, 49,52 and more recent helium tagging infrared photodissociation (IRPD) spectroscopic experiments of Roithová, Costas, and coworkers.53

In contrast, the pentadentate BnTPEN ligand framework forms a terminal S = 1/2 Fe^{III}-OOH species with a coordinately saturated coordination sphere, much like the Cpd 0 species found in heme systems 10,11 and requires the added strong acid to react directly with the Fe^{III}-OOH moiety in an intermolecular fashion. The effects of water on 1catalyzed reactions in the presence of strong acids are drastically different from those found for Fe(TPA). At the same water concentration, the incorporation of water oxygen into cyclohexanol is observed to a much lower extent for 1 compared to [Fe(TPA)(NCCH₃)₂]^{2+,45,46,50} Most significant of all, strong acids greatly accelerate the decay of 2 even at 1 mM ($k_{\rm obs} \sim 1~{\rm s}^{-1}$ at $-40~{\rm ^{\circ}C}$), resulting in decay rates at least 2 orders of magnitude faster than the fastest rate for water-assisted Fe^{III}–OOH decay ($k_{\rm obs}\sim 0.007~{\rm s}^{-1}$ at 300 mM H₂O at -40 °C). 50 However, the presence of 50 equiv of water can slow down the decay of 2 by about 60-fold (Figure S9). These observations clearly establish the proton-assisted O-O bond cleavage pathway of 1 as a separate pathway from the waterassisted pathway.

In this study, we have taken advantage of the pendant benzyl group of the BnTPEN framework as a mechanistic probe for the reactivity of 2, as the hydroxylation of this aromatic ring gives rise to the intramolecular phenolate product 3. Indeed, intramolecular aromatic hydroxylation has been observed for a number of nonheme iron complexes, for which either Fe^{IV}=O or Fe^V=O species are proposed to be the arene hydroxylating agent.^{70–75} In the case of **2**, we can exclude [(BnTPEN)- $Fe^{IV}(O)$]²⁺ as a possibility.^{95,108} Although HAT reactivity has been studied in detail for this complex, 95,108 to the best of our knowledge there is no report that it is capable of intramolecular aromatic hydroxylation. Nam and Fukuzumi have reported that metal-oxo species in the presence of strong protic acids can exhibit enhanced reactivity via a protoncoupled electron transfer (PCET) pathway, 83 and this effect is seen in the oxidation of α -methylstyrene by [(N4Py)-Fe^{IV}(O)]²⁺ in the presence of HOTf. Under our reaction conditions, however, addition of 1 equiv of HClO₄ does not significantly accelerate the decay of [(BnTPEN)Fe^{IV}(O)]²⁺ nor lead to the formation of 3 (Figure S16); even high concentrations of perchloric acid do not accelerate its decay nor is pyridyl arm dissociation found (Figure S17). These observations show that $[(BnTPEN)Fe^{IV}(O)]^{2+}$ is not activated by the presence of strong acids and can be ruled out as the

active species, thus leading us to invoke an Fe^V=O oxidant that is formed by the heterolytic cleavage of the O-O bond in

Thus far, there is only one example, reported by Hitomi and co-workers, that presents substantial evidence for an Fe^V=O species formed in a catalytic nonheme iron system supported by a pentadentate ligand. They have demonstrated hydroxylation of cyclohexane using H₂O₂ with [(DPAQ)- $Fe^{III}(OH_2)]^{2+}$ (DPAQ = 2-[bis(pyridine-2-ylmethyl)]amino-N-quinolin-8-ylacetamidate anion) as the catalyst without requiring any additives. Ions consistent with [(DPAQ)- $\operatorname{Fe}^{\operatorname{III}}(\operatorname{OOH})^{+}$ $(m/z \ 471.1)$ and $\{[(\operatorname{DPAQ})\operatorname{Fe}^{\operatorname{V}}(\operatorname{O})]\operatorname{ClO}_{4}\}^{+}$ (m/z 553.1) have been observed by cryospray ionization mass spectroscopy (CSI-MS). Furthermore, A/K ratios as high as 11 are found for cyclohexane oxidation at room temperature, consistent with metal-based oxidation. In this ligand framework, the introduction of the monoanionic amidate donor lowers the redox potential of the iron center, while its location trans to the hydroperoxo ligand provides a "push" toward heterolytic cleavage of the O-O bond and stabilizes the incipient Fe^V=O oxidant, analogous to the role ascribed to the thiolate ligand in cytochrome P450. 112-114 It is also proposed that the proton released upon H₂O₂ binding to the [(DPAQ)Fe^{III}(OH₂)]²⁺ catalyst provides the "pull" to cleave the O-O bond heterolytically. Unfortunately, these catalytic experiments were carried out at room temperature with the H₂O₂ being delivered by syringe pump over a 30 min period, so there is no kinetic data available with which to compare O-O bond cleavage rates of $[(BnTPEN)Fe^{III}(OOH)]^{2+}$ (2) and [(DPAQ)Fe^{III}(OOH)]⁺. However, given that substrate hydroxylation by 2 is shown to occur at -40 °C within seconds after the introduction of the strong acid, it would seem likely that the O-O bond cleavage step to generate the Fe^V=O oxidant is significantly more facile in the case of 2.

In an effort to demonstrate the feasibility of generating a metastable oxoiron(V) complex, Collins has incorporated four highly electron-donating amido donors into a macrocyclic ligand called TAML, which stands for tetraamido macrocyclic ligand, leading to the characterization of the first bona fide Fe^V=O complex. 115,116 A family of relatively stable (TAML)-Fe^V(O) complexes has been obtained by introducing different substituents on the macrocycle. Perhaps not surprisingly, these complexes exhibit cyclohexane oxidation rates with $k_2 < 10^{-3}$ M^{-1} s⁻¹ at -40 °C, ^{117,118} which are 2 orders of magnitude slower than those found for the two most reactive oxoiron(IV) complexes described to date. ^{119,120} In contrast, cyclohexane oxidation by the putative Fe^V=O oxidant derived from the addition of 1 equiv of HClO₄ to 2 in the presence of cyclohexane occurs within seconds at this temperature. In the latter case, substrate oxidation occurs at a rate independent of substrate concentration, as it takes place subsequent to the rate-determining decay of 2 upon its reaction with strong acids. Thus, substrate oxidation must occur at a rate faster than the reaction of 2 with $HClO_4$. The $k_{\rm obs}$ value for 1 mM 2 and 1 mM HClO₄ is 1.3 s⁻¹ at -40 °C, which is at least 3 orders of magnitude faster than the oxidation rate of 1 M cyclohexane by $[(TAML)Fe^{V}(O)]^{-}$ at -40 °C and 3-5-fold faster than the two most reactive nonheme Fe^{IV}=O complexes reported thus far. 119,120

When the reactivity of 2 in the presence of strong acid is compared with reported rates for cyclohexane oxidation (assuming a substrate concentration of 1 M as used in our catalysis studies), the cyclohexane oxidation rate for 2 is

calculated to be at least an order of magnitude faster than that found for a synthetic Cpd I model, the one-electron oxidized derivative of $[(TDCPP)Fe^{IV}(O)](H_2TDCPP = meso\text{-tetrakis-}$ (2,6-dichlorophenyl)porphin) ($k_{\text{obs}} = 1.1 \times 10^{-1} \text{ s}^{-1}$ for 1 M cyclohexane at -40 °C). 120 However, it is much less reactive than AaeAPO-I, the Cpd I intermediate of a heme-thiolate peroxygenase, which exhibits a $k_{\rm obs}$ of $10^4~{\rm s}^{-1}$ for the oxidation of 1 M cyclohexane carboxylic acid at 4 °C. 121 The rate constant for the decay of 2 in the presence of 1 mM HOTf increases by a factor of 15 when its rate at -40 °C is extrapolated to 4 °C based on an Eyring analysis of its temperature dependence (Figure S13), making it about 3 orders of magnitude less reactive than AaeAPO-I. These comparisons suggest that the oxidant generated from the reaction of 2 with 1 equiv strong acid is a reasonably effective oxidant.

The acid pK_a -dependent nature of the O-O bond cleavage of 2 is particularly intriguing, as it reveals the essential role of a proton in controlling the mode of O-O bond cleavage. This work represents the first systematic study of such effects on Fe^{III}-OOH species in a nonheme iron system. In the heme literature, a study corresponding to our work has been reported by van Eldik and co-workers in aqueous media for an Fe^{III}-OOH species supported by an octa-anionic porphyrin ligand, where it is determined that O-O bond heterolysis of the Fe^{III}-OOH species occurs only when the pH of the aqueous medium is below 8.5.24 Remarkably, this is the same pK_a threshold we have found for the acids capable of eliciting heterolytic cleavage of 2 in CH₃CN (Table 1). While it is difficult to determine the absolute pH values of our reaction mixtures with CH₃CN as the solvent, we would propose that the pH range at which 2 reactivity changes corresponds to the pK_h of the distal OH group of the -OOH ligand, which may be readily protonated upon the addition of sufficiently strong acids to result in O-O bond heterolysis and promote the formation of an Fe^V=O oxidant.

Protons are thus critical participants in both heme and nonheme iron-catalyzed oxidations, indispensable in providing the driving force for O-O bond cleavage to generate highvalent iron species in nature as shown in the formation of Cpd I in heme enzymes⁹⁷ and the diiron(IV) oxidant **Q** in methane monooxygenase for the conversion of methane to methanol. 98,99 In these two cases, O-O bond cleavage to generate the respective key oxidants occurs at comparable pH's and with comparable solvent kinetic isotope effects. Our successful attempt in generating a powerful oxidant, which we propose to be an Fe^V=O species, by proton-assisted O-O bond heterolysis of an Fe^{III}-OOH species also occurs at a similar "pH" in CH3CN. Our bioinspired approach has thus enabled the inherently "sluggish" [(BnTPEN)Fe^{III}(OOH)]²⁺ complex⁴² to perform catalytic cyclohexane hydroxylation with high A/K ratios, an outcome not previously observed for Fe(R-TPEN) complexes in their history of more than 20 years. Given the large reservoir of pentadentate iron complexes, this approach may turn out to be useful for identifying effective catalysts that generate Fe^V=O species as the active oxidant, an aspect whose very surface we have only skimmed.

SAFETY NOTE: 90% H₂O₂ is potentially explosive and should be handled with proper safety precautions. See the Supporting Information for experimental details.

ASSOCIATED CONTENT

S Supporting Information

The Supporting Information is available free of charge on the ACS Publications website at DOI: 10.1021/jacs.9b08442.

Experimental details regarding syntheses, general sample preparation procedures, physical methods, and additional tables and figures (PDF)

AUTHOR INFORMATION

Corresponding Author

*larryque@umn.edu

ORCID ®

Shuangning Xu: 0000-0002-3391-3952 Apparao Draksharapu: 0000-0001-7897-3230

Wagas Rasheed: 0000-0003-3353-9347 Lawrence Que, Jr.: 0000-0002-0989-2813

Present Address

(A.D.) Department of Chemistry, Indian Institute of Technology Kanpur, Kanpur 208016, India.

The authors declare no competing financial interest.

ACKNOWLEDGMENTS

We thank the National Science Foundation for support of this work (CHE1665391 to L.Q.), Prof. John D. Lipscomb for his insightful comments on the kinetic analyses, Prof. Steven R. Kass for helpful discussions on interpreting the H/D isotope effects, and Mr. Jaemin Jung for technical support for the gas chromatography experiments. We also thank the reviewers for their insightful comments and Dr. Caleb J. Allpress for helpful suggestions to address some of the reviewers' concerns.

REFERENCES

- (1) Costas, M.; Mehn, M. P.; Jensen, M. P.; Que, L., Jr. Dioxygen Activation at Mononuclear Nonheme Iron Active Sites: Enzymes, Models, and Intermediates. Chem. Rev. 2004, 104, 939-986.
- (2) Kal, S.; Que, L., Jr. Dioxygen Activation by Nonheme Iron Enzymes with the 2-His-1-Carboxylate Facial Triad that Generate High-Valent Oxoiron Oxidants. JBIC, J. Biol. Inorg. Chem. 2017, 22,
- (3) Jasniewski, A. J.; Que, L., Jr. Dioxygen Activation by Nonheme Diiron Enzymes: Diverse Dioxygen Adducts, High-Valent Intermediates, and Related Model Complexes. Chem. Rev. 2018, 118, 2554-
- (4) Kovaleva, E. G.; Lipscomb, J. D. Versatility of Biological Non-Heme Fe(II) Centers in Oxygen Activation Reactions. Nat. Chem. Biol. 2008, 4, 186-193.
- (5) Guo, M.; Corona, T.; Ray, K.; Nam, W. Heme and Nonheme High-Valent Iron and Manganese Oxo Cores in Biological and Abiological Oxidation Reactions. ACS Cent. Sci. 2019, 5, 13-28.
- (6) Theorell, H. Crystalline Peroxidase. Enzymologia 1942, 10, 250-252.
- (7) Poulos, T. L. Heme Enzyme Structure and Function. Chem. Rev. 2014, 114, 3919-3962.
- (8) Huang, X.; Groves, J. T. Oxygen Activation and Radical Transformations in Heme Proteins and Metalloporphyrins. Chem. Rev. 2018, 118, 2491-2553.
- (9) Denisov, I. G.; Makris, T. M.; Sligar, S. G.; Schlichting, I. Structure and Chemistry of Cytochrome P450. Chem. Rev. 2005, 105, 2253-2278.
- (10) Denisov, I. G.; Mak, P. J.; Makris, T. M.; Sligar, S. G.; Kincaid, J. R. Resonance Raman Characterization of the Peroxo and

- Hydroperoxo Intermediates in Cytochrome P450. J. Phys. Chem. A 2008, 112, 13172–13179.
- (11) Davydov, R.; Hoffman, B. M. Active Intermediates in Heme Monooxygenase Reactions as Revealed by Cryoreduction/Annealing, EPR/ENDOR Studies. *Arch. Biochem. Biophys.* **2011**, *507*, 36–43.
- (12) Kobayashi, K. Pulse Radiolysis Studies for Mechanism in Biochemical Redox Reactions. *Chem. Rev.* **2019**, *119*, 4413–4462.
- (13) Fita, I.; Rossmann, M. G. The Active Center of Catalase. *J. Mol. Biol.* **1985**, *185*, 21–37.
- (14) Poulos, T. L.; Freer, S. T.; Alden, R. A.; Edwards, S. L.; Skogland, U.; Takio, K.; Eriksson, B.; Xuong, N.; Yonetani, T.; Kraut, J. The Crystal Structure of Cytochrome c Peroxidase. *J. Biol. Chem.* 1980, 255, 575–580.
- (15) Sundaramoorthy, M.; Terner, J.; Poulos, T. L. The Crystal Structure of Chloroperoxidase: a Heme Peroxidase–Cytochrome P450 Functional Hybrid. *Structure* **1995**, *3*, 1367–1378.
- (16) Piontek, K.; Strittmatter, E.; Ullrich, R.; Grobe, G.; Pecyna, M. J.; Kluge, M.; Scheibner, K.; Hofrichter, M.; Plattner, D. A. Structural Basis of Substrate Conversion in a New Aromatic Peroxygenase: Cytochrome P450 Functionality with Benefits. *J. Biol. Chem.* **2013**, 288, 34767–34776.
- (17) Lee, D. S.; Yamada, A.; Sugimoto, H.; Matsunaga, I.; Ogura, H.; Ichihara, K.; Adachi, S.; Park, S. Y.; Shiro, Y. Substrate Recognition and Molecular Mechanism of Fatty Acid Hydroxylation by Cytochrome P450 from *Bacillus subtilis*: Crystallographic, Spectroscopic, and Mutational Studies. *J. Biol. Chem.* **2003**, *278*, 9761–9767.
- (18) Belcher, J.; McLean, K. J.; Matthews, S.; Woodward, L. S.; Fisher, K.; Rigby, S. E.; Nelson, D. R.; Potts, D.; Baynham, M. T.; Parker, D. A.; Leys, D.; Munro, A. W. Structure and Biochemical Properties of the Alkene Producing Cytochrome P450 OleT_{JE} (CYP152L1) from the *Jeotgalicoccus* sp. 8456 Bacterium. *J. Biol. Chem.* **2014**, 289, 6535–6550.
- (19) Schlichting, I.; Berendzen, J.; Chu, K.; Stock, A. M.; Maves, S. A.; Benson, D. E.; Sweet, B. M.; Ringe, D.; Petsko, G. A.; Sligar, S. G. The Catalytic Pathway of Cytochrome P450cam at Atomic Resolution. *Science* **2000**, 287, 1615–1622.
- (20) Nagano, S.; Poulos, T. L. Crystallographic Study on the Dioxygen Complex of Wild-Type and Mutant Cytochrome P450cam. Implications for the Dioxygen Activation Mechanism. *J. Biol. Chem.* **2005**, 280, 31659–31663.
- (21) Oszajca, M.; Franke, A.; Brindell, M.; Stochel, G.; van Eldik, R. Redox Cycling in the Activation of Peroxides by Iron Porphyrin and Manganese Complexes. 'Catching' Catalytic Active Intermediates. Coord. Chem. Rev. 2016, 306, 483–509.
- (22) Traylor, T. G.; Xu, F. Mechanisms of Reactions of Iron(III) Porphyrins with Hydrogen-Peroxide and Hydroperoxides Solvent and Solvent Isotope Effects. *J. Am. Chem. Soc.* **1990**, *112*, 178–186.
- (23) Traylor, T. G.; Kim, C.; Richards, J. L.; Xu, F.; Perrin, C. L. Reactions of Iron(III) Porphyrins with Oxidants Structure-Reactivity Studies. *J. Am. Chem. Soc.* **1995**, *117*, 3468–3474.
- (24) Brausam, A.; Eigler, S.; Jux, N.; van Eldik, R. Mechanistic Investigations of the Reaction of an Iron(III) Octa-Anionic Porphyrin Complex with Hydrogen Peroxide and the Catalyzed Oxidation of Diammonium-2,2'-azinobis(3-ethylbenzothiazoline-6-sulfonate). *Inorg. Chem.* **2009**, 48, 7667–7678.
- (25) Jin, N.; Lahaye, D. E.; Groves, J. T. A "Push-Pull" Mechanism for Heterolytic O-O Bond Cleavage in Hydroperoxo Manganese Porphyrins. *Inorg. Chem.* **2010**, *49*, 11516–11524.
- (26) Girerd, J.-J.; Banse, F.; Simaan, A. J., Characterization and Properties of Non-Heme Iron Peroxo Complexes. In *Structure and Bonding (Berlin)*; Meunier, B., Ed.; Springer: Berlin, 2000; pp 145–177.
- (27) Burger, R. M., Nature of Activated Bleomycin. In *Structure and Bonding (Berlin)*; Meunier, B., Ed.; Springer: Berlin, 2000; pp 287–303.
- (28) Burger, R. M.; Peisach, J.; Horwitz, S. B. Activated Bleomycin. A Transient Complex of Drug, Iron, and Oxygen that Degrades DNA. *J. Biol. Chem.* **1981**, 256, 11636–11644.

- (29) Kumar, D.; Hirao, H.; Shaik, S.; Kozlowski, P. M. Proton-Shuffle Mechanism of O-O Activation for Formation of a High-Valent Oxo-Iron Species of Bleomycin. *J. Am. Chem. Soc.* **2006**, *128*, 16148–16158
- (30) Chow, M. S.; Liu, L. V.; Solomon, E. I. Further Insights into the Mechanism of the Reaction of Activated Bleomycin with DNA. *Proc. Natl. Acad. Sci. U. S. A.* **2008**, *105*, 13241–13245.
- (31) Decker, A.; Chow, M. S.; Kemsley, J. N.; Lehnert, N.; Solomon, E. I. Direct Hydrogen-Atom Abstraction by Activated Bleomycin: an Experimental and Computational Study. *J. Am. Chem. Soc.* **2006**, *128*, 4719–4733.
- (32) Solomon, E. I.; Light, K. M.; Liu, L. V.; Srnec, M.; Wong, S. D. Geometric and Electronic Structure Contributions to Function in Non-heme Iron Enzymes. *Acc. Chem. Res.* **2013**, *46*, 2725–2739.
- (33) Bernal, I.; Jensen, I. M.; Jensen, K. B.; McKenzie, C. J.; Toftlund, H.; Tuchagues, J.-P. Iron(II) Complexes of Polydentate Aminopyridyl Ligands and an Exchangeable Sixth Ligand; Reactions with Peroxides. Crystal Structure of [FeL¹(H₂O)][PF₆]₂·H₂O [L¹=N,N'-bis-(6-methyl-2-pyridylmethyl)-N,N'-bis(2-pyridylmethyl)-ethane-1,2-diamine]. *J. Chem. Soc., Dalton Trans.* 1995, 3667–3675.
- (34) Lubben, M.; Meetsma, A.; Wilkinson, E. C.; Feringa, B.; Que, L., Jr. Nonheme Iron Centers in Oxygen Activation Characterization of an Iron(III) Hydroperoxide Intermediate. *Angew. Chem., Int. Ed. Engl.* 1995, 34, 1512–1514.
- (35) Hazell, A.; McKenzie, C. J.; Nielsen, L. P.; Schindler, S.; Weitzer, M. Mononuclear Non-Heme Iron(III) Peroxide Complexes: Syntheses, Characterisation, Mass Spectrometric and Kinetic Studies. *J. Chem. Soc., Dalton Trans.* **2002**, 310–317.
- (36) Koehntop, K. D.; Rohde, J.-U.; Costas, M.; Que, L., Jr. XAS Characterization of End-On and Side-On Peroxoiron(III) Complexes of the Neutral Pentadentate N-Donor Ligand N-methyl-N,N',N'-tris(2-pyridylmethyl)ethane-1,2-diamine. *Dalton Trans.* **2004**, 3191–3198.
- (37) Martinho, M.; Dorlet, P.; Riviere, E.; Thibon, A.; Ribal, C.; Banse, F.; Girerd, J. J. Preparation and Characterization of a Microcrystalline Non-Heme Fe^{III}(OOH) Complex Powder: EPR Reinvestigation of Fe^{III}(OOH) Complexes-Improvement of the Perturbation Equations for the *g* Tensor of Low-Spin Fe^{III}. *Chem. Eur. J.* **2008**, *14*, 3182–3188.
- (38) Hong, S.; Lee, Y.-M.; Shin, W.; Fukuzumi, S.; Nam, W. Dioxygen Activation by Mononuclear Nonheme Iron(II) Complexes Generates Iron—Oxygen Intermediates in the Presence of an NADH Analogue and Proton. *J. Am. Chem. Soc.* **2009**, *131*, 13910—13911.
- (39) Faponle, A. S.; Quesne, M. G.; Sastri, C. V.; Banse, F.; de Visser, S. P. Differences and Comparisons of the Properties and Reactivities of Iron(III)—Hydroperoxo Complexes with Saturated Coordination Sphere. *Chem. Eur. J.* 2015, 21, 1221–1236.
- (40) Faponle, A. S.; Banse, F.; de Visser, S. P. Arene Activation by a Nonheme Iron(III)—Hydroperoxo Complex: Pathways Leading to Phenol and Ketone Products. *JBIC, J. Biol. Inorg. Chem.* **2016**, 21, 453–462.
- (41) Hölzl, S. M.; Altmann, P. J.; Kuck, J. W.; Kuhn, F. E. Speciation in Iron Epoxidation Catalysis: A Perspective on the Discovery and Role of Non-Heme Iron(III)-Hydroperoxo Species in Iron-Catalyzed Oxidation Reactions. *Coord. Chem. Rev.* **2017**, 352, 517–536.
- (42) Park, M. J.; Lee, J.; Suh, Y.; Kim, J.; Nam, W. Reactivities of Mononuclear Non-Heme Iron Intermediates Including Evidence that Iron(III)-Hydroperoxo Species is a Sluggish Oxidant. *J. Am. Chem. Soc.* **2006**, *128*, 2630–2634.
- (43) Roelfes, G.; Lubben, M.; Hage, R.; Que, L., Jr.; Feringa, B. L. Catalytic Oxidation with a Non-Heme Iron Complex That Generates a Low-Spin Fe^{III}OOH Intermediate. *Chem. Eur. J.* **2000**, *6*, 2152–2159.
- (44) Chen, J.; Draksharapu, A.; Angelone, D.; Unjaroen, D.; Padamati, S. K.; Hage, R.; Swart, M.; Duboc, C.; Browne, W. R. H₂O₂ Oxidation by Fe(III)—OOH Intermediates and Its Effect on Catalytic Efficiency. *ACS Catal.* **2018**, *8*, 9665—9674.

- (45) Chen, K.; Que, L., Jr. Stereospecific Alkane Hydroxylation by Non-Heme Iron Catalysts: Mechanistic Evidence for an Fe^VO Active Species. *J. Am. Chem. Soc.* **2001**, *123*, 6327–6337.
- (46) Chen, K.; Costas, M.; Kim, J.; Tipton, A. K.; Que, L., Jr. Olefin Cis-Dihydroxylation versus Epoxidation by Non-Heme Iron Catalysts: Two Faces of an Fe^{III}–OOH Coin. *J. Am. Chem. Soc.* **2002**, *124*, 3026–3035.
- (47) Company, A.; Gomez, L.; Guell, M.; Ribas, X.; Luis, J. M.; Que, L., Jr.; Costas, M. Alkane Hydroxylation by a Nonheme Iron Catalyst that Challenges the Heme Paradigm for Oxygenase Action. *J. Am. Chem. Soc.* **2007**, *129*, 15766–15767.
- (48) Prat, I.; Mathieson, J. S.; Guell, M.; Ribas, X.; Luis, J. M.; Cronin, L.; Costas, M. Observation of Fe(V)=O using Variable-Temperature Mass Spectrometry and Its Enzyme-Like C-H and C = C Oxidation Reactions. *Nat. Chem.* **2011**, *3*, 788–793.
- (49) Prat, I.; Company, A.; Postils, V.; Ribas, X.; Que, L., Jr.; Luis, J. M.; Costas, M. The Mechanism of Stereospecific C-H Oxidation by Fe(Pytacn) Complexes: Bioinspired Non-Heme Iron Catalysts Containing *cis*-Labile Exchangeable Sites. *Chem. Eur. J.* **2013**, 19, 6724–6738.
- (50) Oloo, W. N.; Fielding, A. J.; Que, L., Jr. Rate-Determining Water-Assisted O–O Bond Cleavage of an Fe^{III}–OOH Intermediate in a Bio-inspired Nonheme Iron-Catalyzed Oxidation. *J. Am. Chem. Soc.* **2013**. *135*. 6438–6441.
- (51) Oloo, W. N.; Que, L., Jr. Bioinspired Nonheme Iron Catalysts for C-H and C = C Bond Oxidation: Insights into the Nature of the Metal-Based Oxidants. *Acc. Chem. Res.* **2015**, *48*, 2612–2621.
- (52) Xu, S.; Veach, J. J.; Oloo, W. N.; Peters, K. C.; Wang, J.; Perry, R. H.; Que, L., Jr. Detection of a Transient Fe(V)(O)(OH) Species Involved in Olefin Oxidation by a Bio-Inspired Non-Haem Iron Catalyst. *Chem. Commun.* **2018**, *54*, 8701–8704.
- (53) Borrell, M.; Andris, E.; Navrátil, R.; Roithová, J.; Costas, M. Characterized *cis*-FeV(O)(OH) Intermediate Mimics Enzymatic Oxidations in the Gas Phase. *Nat. Commun.* **2019**, *10*, 901.
- (54) Kal, S.; Xu, S.; Que, L. Bio-inspired Nonheme Iron Oxidation Catalysis. Growing Evidence for the Involvement of Oxoiron(V) Oxidants in Cleaving Strong C–H Bonds. *Angew. Chem., Int. Ed.* **2019**, DOI: 10.1002/anie.201906551.
- (55) Serrano-Plana, J.; Acuna-Pares, F.; Dantignana, V.; Oloo, W. N.; Castillo, E.; Draksharapu, A.; Whiteoak, C. J.; Martin-Diaconescu, V.; Basallote, M. G.; Luis, J. M.; Que, L., Jr.; Costas, M.; Company, A. Acid-Triggered O-O Bond Heterolysis of a Nonheme Fe(III)(OOH) Species for the Stereospecific Hydroxylation of Strong C-H Bonds. *Chem. Eur. J.* 2018, 24, 5331–5340.
- (56) Kal, S.; Draksharapu, A.; Que, L., Jr. Sc³⁺ (or HClO₄) Activation of a Nonheme Fe^{III}–OOH Intermediate for the Rapid Hydroxylation of Cyclohexane and Benzene. *J. Am. Chem. Soc.* **2018**, *140*, 5798–5804.
- (57) Jensen, K. B.; McKenzie, C. J.; Nielsen, L. P.; Zacho Pedersen, J.; Svendsen, H. M. Deprotonation of Low-Spin Mononuclear Iron(III)—Hydroperoxide Complexes Give Transient Blue Species Assigned to High-Spin Iron(III)—Peroxide Complexes. *Chem. Commun.* 1999, 1313—1314.
- (58) Thibon, A.; Jollet, V.; Ribal, C.; Senechal-David, K.; Billon, L.; Sorokin, A. B.; Banse, F. Hydroxylation of Aromatics with the Help of a Non-Haem FeOOH: a Mechanistic Study under Single-Turnover and Catalytic Conditions. *Chem. Eur. J.* **2012**, *18*, 2715–2724.
- (59) Ortega-Villar, N.; Ugalde-Saldívar, V. M.; Muñoz, M. C.; Ortiz-Frade, L. A.; Alvarado-Rodríguez, J. G.; Real, J. A.; Moreno-Esparza, R. Synthesis and Relative Stability of a Series of Compounds of Type [Fe(II)(bztpen)X]+, Where bztpen = Pentadentate Ligand, N5, and X- = Monodentate Anion. *Inorg. Chem.* **2007**, *46*, 7285–7293.
- (60) Rohde, J.-U.; Torelli, S.; Shan, X.; Lim, M. H.; Klinker, E. J.; Kaizer, J.; Chen, K.; Nam, W.; Que, L. Structural Insights into Nonheme Alkylperoxoiron(III) and Oxoiron(IV) Intermediates by X-ray Absorption Spectroscopy. *J. Am. Chem. Soc.* **2004**, *126*, 16750–16761
- (61) Draksharapu, A.; Li, Q.; Logtenberg, H.; van den Berg, T. A.; Meetsma, A.; Killeen, J. S.; Feringa, B. L.; Hage, R.; Roelfes, G.;

- Browne, W. R. Ligand Exchange and Spin State Equilibria of Fe(II)(N4Py) and Related Complexes in Aqueous Media. *Inorg. Chem.* **2012**, *51*, 900–13.
- (62) Ligtenbarg, A. G. J.; Oosting, P.; Roelfes, G.; Crois, R. M. L.; Lutz, M.; Spek, A. L.; Hage, R.; Feringa, B. L. Efficient Catalytic Oxidation of Primary and Secondary Alcohols Using a Non-Heme Dinuclear Iron Complex. *Chem. Commun.* **2001**, 385–386.
- (63) Unjaroen, D.; Swart, M.; Browne, W. R. Electrochemical Polymerization of Iron(III) Polypyridyl Complexes through C–C Coupling of Redox Non-innocent Phenolato Ligands. *Inorg. Chem.* **2017**, *56*, 470–479.
- (64) Michaud-Soret, I.; Andersson, K. K.; Que, L., Jr.; Haavik, J. Resonance Raman Studies of Catecholate and Phenolate Complexes of Recombinant Human Tyrosine Hydroxylase. *Biochemistry* **1995**, *34*, 5504–5510.
- (65) Pyrz, J. W.; Roe, A. L.; Stern, L. J.; Que, L., Jr. Model Studies of Iron Tyrosinate Proteins. J. Am. Chem. Soc. 1985, 107, 614–620.
- (66) Que, L., Jr. Metalloproteins with Phenolate Coordination. Coord. Chem. Rev. 1983, 50, 73–108.
- (67) Gaber, B. P.; Miskowski, V.; Spiro, T. G. Resonance Raman Scattering from Iron(III)- and Copper(II)-Transferrin and an Iron(III) Model Compound. Spectroscopic Interpretation of the Transferrin Binding Site. *J. Am. Chem. Soc.* **1974**, *96*, 6868–6873.
- (68) Ahrland, S.; Dahlgren, Å.; Persson, I. Stabilities and Hydrolysis of Some Iron(III) and Manganese(III) Complexes with Chelating Ligands. *Acta Agric. Scand.* **1990**, *40*, 101–111.
- (69) Gómez-Gallego, M.; Sierra, M. A.; Alcázar, R.; Ramírez, P.; Piñar, C.; Mancheño, M. J.; García-Marco, S.; Yunta, F.; Lucena, J. J. Synthesis of *o,p*-EDDHA and Its Detection as the Main Impurity in *o,o*-EDDHA Commercial Iron Chelates. *J. Agric. Food Chem.* **2002**, *50*, 6395–6399.
- (70) Mehn, M. P.; Fujisawa, K.; Hegg, E. L.; Que, L., Jr. Oxygen Activation by Nonheme Iron(II) Complexes: α -Keto Carboxylate versus Carboxylate. *J. Am. Chem. Soc.* **2003**, *125*, 7828–7842.
- (71) Jensen, M. P.; Lange, S. J.; Mehn, M. P.; Que, E. L.; Que, L., Jr. Biomimetic Aryl Hydroxylation Derived from Alkyl Hydroperoxide at a Nonheme Iron Center. Evidence for an Fe^{IV}O Oxidant. *J. Am. Chem. Soc.* **2003**, *125*, 2113–2128.
- (72) Nielsen, A.; Larsen, F. B.; Bond, A. D.; McKenzie, C. J. Regiospecific Ligand Oxygenation in Iron Complexes of a Carboxylate-Containing Ligand Mediated by a Proposed FeV-Oxo Species. *Angew. Chem., Int. Ed.* **2006**, 45, 1602–1606.
- (73) Sahu, S.; Widger, L. R.; Quesne, M. G.; de Visser, S. P.; Matsumura, H.; Moënne-Loccoz, P.; Siegler, M. A.; Goldberg, D. P. Secondary Coordination Sphere Influence on the Reactivity of Nonheme Iron(II) Complexes: An Experimental and DFT Approach. *J. Am. Chem. Soc.* **2013**, 135, 10590–10593.
- (74) Sahu, S.; Quesne, M. G.; Davies, C. G.; Dürr, M.; Ivanović-Burmazović, I.; Siegler, M. A.; Jameson, G. N. L.; de Visser, S. P.; Goldberg, D. P. Direct Observation of a Nonheme Iron(IV)—Oxo Complex That Mediates Aromatic C—F Hydroxylation. *J. Am. Chem. Soc.* 2014, 136, 13542—13545.
- (75) Sahu, S.; Zhang, B.; Pollock, C. J.; Dürr, M.; Davies, C. G.; Confer, A. M.; Ivanović-Burmazović, I.; Siegler, M. A.; Jameson, G. N. L.; Krebs, C.; Goldberg, D. P. Aromatic C–F Hydroxylation by Nonheme Iron(IV)—Oxo Complexes: Structural, Spectroscopic, and Mechanistic Investigations. *J. Am. Chem. Soc.* **2016**, *138*, 12791—12802
- (76) Luo, Y.-R. Comprehensive Handbook of Chemical Bond Energies; CRC Press: Boca Raton, FL, 2007.
- (77) Kim, J.; Harrison, R. G.; Kim, C.; Que, L., Jr. Fe(TPA)-Catalyzed Alkane Hydroxylation. Metal-Based Oxidation vs Radical Chain Autoxidation. *J. Am. Chem. Soc.* **1996**, *118*, 4373–4379.
- (78) Russell, G. A. Deuterium-isotope Effects in the Autoxidation of Aralkyl Hydrocarbons. Mechanism of the Interaction of Peroxy Radicals. J. Am. Chem. Soc. 1957, 79, 3871–3877.
- (79) Eckert, F.; Leito, I.; Kaljurand, I.; Kutt, A.; Klamt, A.; Diedenhofen, M. Prediction of Acidity in Acetonitrile Solution with COSMO-RS. *J. Comput. Chem.* **2009**, *30*, 799–810.

- (80) Lokov, M.; Tshepelevitsh, S.; Heering, A.; Plieger, P. G.; Vianello, R.; Leito, I. On the Basicity of Conjugated Nitrogen Heterocycles in Different Media. Eur. J. Org. Chem. 2017, 2017, 4475-4489.
- (81) Chen, K.; Que, L., Jr. Evidence for the Participation of a High-Valent Iron-Oxo Species in Stereospecific Alkane Hydroxylation by a Non-Heme Iron Catalyst. Chem. Commun. 1999, 1375-1376.
- (82) Wegeberg, C.; Lauritsen, F. R.; Frandsen, C.; Morup, S.; Browne, W. R.; McKenzie, C. J. Directing a Non-Heme Iron(III)-Hydroperoxide Species on a Trifurcated Reactivity Pathway. Chem. -Eur. J. 2018, 24, 5134-5145.
- (83) Sénéchal-David, K.; Buron, C.; Ségaud, N.; Rebilly, J.-N.; Dos Santos, A.; Farjon, J.; Guillot, R.; Herrero, C.; Inceoglu, T.; Banse, F. Non-Heme Fe(II) Diastereomeric Complexes Bearing a Hexadentate Ligand: Unexpected Consequences on the Spin State and Oxidation Catalytic Properties. Chem. - Eur. J. 2019, 25, 12405.
- (84) Wegeberg, C.; Browne, W. R.; McKenzie, C. J. cis Donor Influence on O-O Bond Lability in Iron(III) Hydroperoxo Complexes: Oxidation Catalysis and Ligand Transformation. Inorg. Chem. 2019, 58, 8983-8994.
- (85) Lyakin, O. Y.; Bryliakov, K. P.; Talsi, E. P. Non-Heme Oxoiron(V) Intermediates in Chemo-, Regio- and Stereoselective Oxidation of Organic Substrates. Coord. Chem. Rev. 2019, 384, 126-
- (86) Capocasa, G.; Olivo, G.; Barbieri, A.; Lanzalunga, O.; Di Stefano, S. Direct Hydroxylation of Benzene and Aromatics with H₂O₂ Catalyzed by a Self-Assembled Iron Complex: Evidence for a Metal-Based Mechanism. Catal. Sci. Technol. 2017, 7, 5677-5686.
- (87) Wolfsberg, M. Theoretical Evaluation of Experimentally Observed Isotope Effects. Acc. Chem. Res. 1972, 5, 225-233.
- (88) Hanzlik, R. P.; Shearer, G. O. Secondary Deuterium Isotope Effects on Olefin Epoxidation by Cytochrome P-450. Biochem. Pharmacol. 1978, 27, 1441-1444.
- (89) de Visser, S. P.; Oh, K.; Han, A. R.; Nam, W. Combined Experimental and Theoretical Study on Aromatic Hydroxylation by Mononuclear Nonheme Iron(IV)-Oxo Complexes. Inorg. Chem. 2007, 46, 4632-4641.
- (90) Makhlynets, O. V.; Rybak-Akimova, E. V. Aromatic Hydroxylation at a Non-Heme Iron Center: Observed Intermediates and Insights into the Nature of the Active Species. Chem. - Eur. J. 2010, 16, 13995-14006.
- (91) Raba, A.; Cokoja, M.; Herrmann, W. A.; Kühn, F. E. Catalytic Hydroxylation of Benzene and Toluene by an Iron Complex Bearing a Chelating Di-pyridyl-di-NHC Ligand. Chem. Commun. 2014, 50,
- (92) Lindhorst, A. C.; Haslinger, S.; Kühn, F. E. Molecular Iron Complexes as Catalysts for Selective C-H Bond Oxygenation Reactions. Chem. Commun. 2015, 51, 17193-17212.
- (93) Lyakin, O. Y.; Zima, A. M.; Tkachenko, N. V.; Bryliakov, K. P.; Talsi, E. P. Direct Evaluation of the Reactivity of Nonheme Iron(V)-Oxo Intermediates toward Arenes. ACS Catal. 2018, 8, 5255-5260.
- (94) Kudrik, E. V.; Sorokin, A. B. N-Bridged Diiron Phthalocyanine Catalyzes Oxidation of Benzene with H2O2 via Benzene Oxide with NIH Shift Evidenced by Using 1,3,5-[D₃]Benzene as a Probe. Chem. -Eur. J. 2008, 14, 7123-7126.
- (95) Kaizer, J.; Klinker, E. J.; Oh, N. Y.; Rohde, J. U.; Song, W. J.; Stubna, A.; Kim, J.; Münck, E.; Nam, W.; Que, L., Jr. Nonheme Fe^{IV}O Complexes That Can Oxidize the C-H bonds of Cyclohexane at Room Temperature. J. Am. Chem. Soc. 2004, 126, 472-473.
- (96) Oloo, W. N.; Banerjee, R.; Lipscomb, J. D.; Que, L., Jr. Equilibrating (L)Fe(III)-OOAc and (L)Fe(V)(O) Species in Hydrocarbon Oxidations by Bio-Inspired Nonheme Iron Catalysts Using H₂O₂ and AcOH. J. Am. Chem. Soc. 2017, 139, 17313-17326.
- (97) Dunford, H. B.; Hewson, W. D.; Steiner, H. Horseradish Peroxidase. XXIX. Reactions in Water and Deuterium Oxide: Cyanide Binding, Compound I Formation, and Reactions of Compounds I and II with Ferrocyanide. Can. J. Chem. 1978, 56, 2844-2852.
- (98) Lee, S. K.; Lipscomb, J. D. Oxygen Activation Catalyzed by Methane Monooxygenase Hydroxylase Component: Proton Delivery

- during the O-O bond Cleavage Steps. Biochemistry 1999, 38, 4423-
- (99) Tinberg, C. E.; Lippard, S. J. Revisiting the Mechanism of Dioxygen Activation in Soluble Methane Monooxygenase from M. capsulatus (Bath): Evidence for a Multi-Step, Proton-Dependent Reaction Pathway. Biochemistry 2009, 48, 12145-12158.
- (100) Purlee, E. L. On the Solvent Isotope Effect of Deuterium in Aqueous Acid Solutions. J. Am. Chem. Soc. 1959, 81, 263-272.
- (101) Gardner Swain, C.; Bader, R. F. W. The Nature of the Structure Difference between Light and Heavy Water and the Origin of the Solvent Isotope Effect—I. Tetrahedron 1960, 10, 182-199.
- (102) Gardner Swain, C.; Bader, R. F. W.; Thornton, E. R. A Theoretical Interpretation of Isotope Effects in Mixtures of Light and Heavy Water-II. Tetrahedron 1960, 10, 200-211.
- (103) Liu, L. V.; Hong, S.; Cho, J.; Nam, W.; Solomon, E. I. Comparison of High-Spin and Low-Spin Nonheme Fe(III)-OOH Complexes in O-O bond Homolysis and H-Atom Abstraction Reactivities. J. Am. Chem. Soc. 2013, 135, 3286-3299.
- (104) Zhang, Q.; Goldsmith, C. R. Kinetic Analysis of the Formation and Decay of a Non-Heme Ferric Hydroperoxide Species Susceptible to O-O Bond Homolysis. Inorg. Chem. 2014, 53, 5206-5211.
- (105) Kaizer, J.; Costas, M.; Que, L., Jr. A Dramatic Push Effect on the Homolysis of Fe^{III}(OOR) Intermediates to Form Non-Heme Fe^{IV}=O Complexes. Angew. Chem., Int. Ed. 2003, 42, 3671–3673.
- (106) Mairata i Payeras, A.; Ho, R. Y.; Fujita, M.; Que, L., Jr. The Reaction of [Fe^{II}(tpa)] with H₂O₂ in Acetonitrile and Acetone-Distinct Intermediates and Yet Similar Catalysis. Chem. - Eur. J. 2004, 10, 4944-4953.
- (107) Li, F.; Meier, K. K.; Cranswick, M. A.; Chakrabarti, M.; Van Heuvelen, K. M.; Münck, E.; Que, L., Jr. Characterization of a High-Spin Non-Heme Fe(III)-OOH Intermediate and Its Quantitative Conversion to an Fe(IV)=O Complex. J. Am. Chem. Soc. 2011, 133, 7256-7259.
- (108) Wang, D.; Ray, K.; Collins, M. J.; Farquhar, E. R.; Frisch, J. R.; Gómez, L.; Jackson, T. A.; Kerscher, M.; Waleska, A.; Comba, P.; Costas, M.; Que, L., Jr. Nonheme Oxoiron(IV) Complexes of Pentadentate N5 Ligands: Spectroscopy, Electrochemistry, and Oxidative Reactivity. Chem. Sci. 2013, 4, 282-291.
- (109) Park, J.; Lee, Y.-M.; Ohkubo, K.; Nam, W.; Fukuzumi, S. Efficient Epoxidation of Styrene Derivatives by a Nonheme Iron(IV)-Oxo Complex via Proton-Coupled Electron Transfer with Triflic Acid. Inorg. Chem. 2015, 54, 5806-5812.
- (110) Nam, W.; Lee, Y.-M.; Fukuzumi, S. Hydrogen Atom Transfer Reactions of Mononuclear Nonheme Metal-Oxygen Intermediates. Acc. Chem. Res. 2018, 51, 2014-2022.
- (111) Hitomi, Y.; Arakawa, K.; Funabiki, T.; Kodera, M. An Iron(III)-Monoamidate Complex Catalyst for Selective Hydroxylation of Alkane C-H Bonds with Hydrogen Peroxide. Angew. Chem., Int. Ed. 2012, 51, 3448-3452.
- (112) Green, M. T.; Dawson, J. H.; Gray, H. B. Oxoiron(IV) in Chloroperoxidase Compound II Is Basic: Implications for P450 Chemistry. Science 2004, 304, 1653-1656.
- (113) Yosca, T. H.; Rittle, J.; Krest, C. M.; Onderko, E. L.; Silakov, A.; Calixto, J. C.; Behan, R. K.; Green, M. T. Iron(IV)hydroxide p K_a and the Role of Thiolate Ligation in C-H Bond Activation by Cytochrome P450. Science 2013, 342, 825-829.
- (114) Groves, J. T. Enzymatic C-H Bond Activation: Using Push to Get Pull. Nat. Chem. 2014, 6, 89-91.
- (115) Collins, T. J.; Ryabov, A. D. Targeting of High-Valent Iron-TAML Activators at Hydrocarbons and Beyond. Chem. Rev. 2017, 117, 9140-9162.
- (116) de Oliveira, F. T.; Chanda, A.; Banerjee, D.; Shan, X.; Mondal, S.; Que, L., Jr.; Bominaar, E. L.; Münck, E.; Collins, T. J. Chemical and Spectroscopic Evidence for an FeV-Oxo Complex. Science 2007, 315, 835-838.
- (117) Kundu, S.; Thompson, J. V. K.; Shen, L. Q.; Mills, M. R.; Bominaar, E. L.; Ryabov, A. D.; Collins, T. J. Activation Parameters as Mechanistic Probes in the TAML Iron(V)-Oxo Oxidations of Hydrocarbons. Chem. - Eur. J. 2015, 21, 1803-1810.

- (118) Ren, Q.; Guo, Y.; Mills, M. R.; Ryabov, A. D.; Collins, T. J. On the Iron(V) Reactivity of an Aggressive Tail-Fluorinated Tetraamido Macrocyclic Ligand (TAML) Activator. *Eur. J. Inorg. Chem.* **2015**, 2015, 1445–1452.
- (119) Biswas, A. N.; Puri, M.; Meier, K. K.; Oloo, W. N.; Rohde, G. T.; Bominaar, E. L.; Münck, E.; Que, L., Jr. Modeling TauD-J: a High-Spin Nonheme Oxoiron(IV) Complex with High Reactivity toward C-H Bonds. *J. Am. Chem. Soc.* **2015**, *137*, 2428–2431.
- (120) Seo, M. S.; Kim, N. H.; Cho, K.-B.; So, J. E.; Park, S. K.; Clémancey, M.; Garcia-Serres, R.; Latour, J.-M.; Shaik, S.; Nam, W. A Mononuclear Nonheme Iron(IV)-Oxo Complex which is More Reactive than Cytochrome P450 Model Compound I. *Chem. Sci.* **2011**, *2*, 1039–1045.
- (121) Wang, X.; Peter, S.; Kinne, M.; Hofrichter, M.; Groves, J. T. Detection and Kinetic Characterization of a Highly Reactive Heme—Thiolate Peroxygenase Compound I. *J. Am. Chem. Soc.* **2012**, *134*, 12897—12900.